DOI: 10.1590/2317-4889201720170068

ARTICLE

Mineralogy, stable isotopes ($\delta^{18}O$ and $\delta^{34}S$) and ^{40}Ar-^{39}Ar geochronology studies on the hydrothermal carapace of the Igarapé Manteiga W-Sn Deposit, Rondônia

Estudos de mineralogia, isótopos estáveis ($\delta^{18}O$ e $\delta^{34}S$) e geocronologia ^{40}Ar-^{39}Ar sobre a carapaça hidrotermal do depósito de W-Sn Igarapé Manteiga, Rondônia

Thais Marcela Fernandes do Nascimento[1], Valmir da Silva Souza[1,2]*

ABSTRACT: The Igarapé Manteiga W-Sn deposit is formed by a granite stock that intrudes in the Paleoproterozoic basement. The mineralization is encapsulated in an alumino-siliceous hydrothermal carapace formed by greisen, vein-veinlets and breccia, developed in the apex zone of a granite stock. At this site, wolframite, cassiterite and sulfides-minerals, as well as siderite, monazite, xenotime, hematite and others, are spread out or in massive clusters associated with quartz, topaz, zinnwaldite and fluorite. Wolframite is not zoned and relatively rich in Fe, and poor in Nb and Ta. Cassiterite exhibits growth-zones with light-yellow to dark-orange colors, and is rich in Ta, and poor in Ti, W, Mn and U. Oxygen and sulfur ($\delta^{18}O$ and $\delta^{34}S$) isotope data on the ore- and sulfide-minerals indicates that it is a magmatic source, with closing temperatures from 230°C to 480°C. The hydrothermal phase was cyclical and protractedly active, promoting greisenization and hydrofracturing. The lowering of temperature and the change in the composition of fluids (from oxidized to reduced) controlled the precipitation of the hydrothermal mineral assemblage. The ^{40}Ar-^{39}Ar analyses reveal a plateau age of 988 Ma, interpreted as the closure time for the hydrothermal processes responsible for mineralization, which is linked to the final magmatic evolution of the Rondônia Intrusive Suite (995-991 Ma).

KEYWORDS: Rondônia Tin Province; Igarapé Manteiga W-Sn deposit; ^{40}Ar-^{39}Ar geochronology; Stable isotope; Mineralogy.

RESUMO: *O depósito de W-Sn Igarapé Manteiga é formado por um stock granítico intrusivo no embasamento Paleoproterozóico. A mineralização está encapsulada em uma carapaça hidrotermal alumino-silicosa formada por greisen, veios-vênulas e brecha, desenvolvidos na zona apical do stock granítico. Os minerais de minério (wolframita ± cassiterita) e minerais sulfetados, bem como siderita, monazita, xenotima, hematita e outros, ocorrem disseminados ou em aglomerados maciços associados com quartzo, topázio, zinnwaldita e fluorita. A wolframita não está zonada, é relativamente rica em Fe, pobre em Nb e Ta, enquanto a cassiterita exibe zonas de crescimento com cores de amarelo claro a laranja escuro, sendo rica em Ta, pobre em Ti, W, Mn e U. Dados de isótopos de oxigênio e enxofre ($\delta^{18}O$ e $\delta^{34}S$) do minério e alguns sulfetos indicam uma fonte magmática, com temperatura de fechamento de 230° a 480°C. A fase hidrotermal foi cíclica e prolongadamente ativa, promovendo greisenização e hidrofraturamento. A diminuição da temperatura e a alteração na composição dos fluidos (de oxidado para reduzido), controlou a precipitação da associação mineral hidrotermal. Análises ^{40}Ar-^{39}Ar revelaram uma idade platô de 988 Ma, interpretada como fechamento do processo hidrotermal responsável pela mineralização, o qual está vinculado à evolução magmática final da Suíte Intrusiva de Rondônia (995-991 Ma).*

PALAVRAS-CHAVE: *Província Estanífera de Rondônia; Depósito de W-Sn Igarapé Manteiga; Geocronologia ^{40}Ar-^{39}Ar; Isótopos estáveis; Mineralogia.*

[1]Geosciences Postgraduate Program, Universidade Federal do Amazonas – UFAM, Manaus (AM), Brazil. *E-mail: thais.marcela@gmail.com*

[2]Geosciences Institute, Universidade de Brasília – IG-UnB, Brasília (DF), Brazil. *E-mail: valmirsouzaunb@gmail.com*

*Corresponding author

Manuscript ID: 20170068. **Received on:** 05/08/2017. **Approved on:** 08/23/2017.

INTRODUCTION

The State of Rondônia, located on the SW border of the Amazonian Craton in Brazil, hosts several Meso- to Neoproterozoic rapakivi granitic associations, which form the Rondônia Tin Province. These granitic suites have A-type and within-plate to post-collisional geochemical signatures, which were emplaced during successive magmatic episodes that occurred between 1606 and 974 Ma (Kloosterman 1968, Priem *et al.* 1966, 1971, Leal *et al.* 1978, Isotta *et al.* 1978, Bettencourt *et al.* 1999, CPRM 2007). However, the most significant metal concentrations (Sn, W, Nb, Ta), as well as F and gemstones, are associated with the last three magmatic episodes that occurred between 1314 and 974 Ma, which are represented by regional units known as the São Lourenço-Caripunas (1314-1309 Ma), Santa Clara (1082-1074 Ma), and Rondônia (995-991 Ma) intrusive suites.

The mineralized sites are distributed mostly in the north-central part of the Rondônia Tin Province and are associated with the Rondônia intrusive suite (Fig. 1). They occupy the apex zone of polyphasic magmatic systems that are linked to late- to post-magmatic hydrothermal phases, encapsulated in hydrothermal carapaces formed by greisen, veins, breccia and pegmatite bodies (Leite Jr. 2002, Souza 2003, Sparrenberger 2003, Bettencourt *et al.* 2005a). However, important mineralized sites also occur in paleo-placer deposits, which have been exploited through a type of artisanal mining known as "garimpo" in Brazil.

The magmatic system of the Igarapé Manteiga W-Sn deposit is linked to the Rondônia intrusive suite (Nascimento 2010). This deposit was discovered in the early 2000s and during 2003-2008, it produced around 5,000 tons/ore (70% wolframite and 30% cassiterite). This mineralization is associated with greisen, vein-veinlets and breccia, but important metal concentrations are also present in paleo-alluvial deposits. However, the 2008 global economic crisis has paralyzed metal extraction. Currently, the METALMIG Mining Company holds the mining rights and is seeking negotiations in order to reopen the mine.

Despite the knowledge gained about tin and other metal deposits in Rondônia (Yokoi *et al.* 1987, Leite Jr. 2002, Souza 2003, Sparrenberger 2003, Bettencourt *et al.* 2005a, Santos Jr. 2015), investigations into the chemical composition, the stable isotopes and the contents of the fluid inclusions in the ore minerals, are still limited. The present paper describes the textural relationships, the chemical and isotopic ($\delta^{18}O$ and $\delta^{34}S$) composition, and the age of the ^{40}Ar-^{39}Ar on the mineralogical association found in the hydrothermal carapace zone of the Igarapé Manteiga W-Sn deposit. Thus, this work aims to characterize substitution mechanisms, chemical and zoning patterns, as well as source and temperature information on these minerals, in order to aid in the understanding of the metallogenic processes that occurred in the north-central part of the Rondônia Tin Province.

METHODS

The conventional petrography was carried out at the Federal University of Amazonas, while the electron microscopy investigation was carried out at the Emílio Goeldi Paraense museum in Brazil, under the supervision of Professor H. T. Costi. A LEO 1450 VP model electron microscope was used on the polished rock sections studied, which were covered by a gold film. This microscope is equipped with a high-performance Gresham EDS/SDD spectrometer system. Mineral imaging was done by acquiring the mixed signal of back-scattered (BSE) and transmitted (TE) electrons. The electrons spectra are acquired at a working distance of 10 mm for 10-20 s of clock time. The probe sizes varied between 0.1-0.2 nm and had a beam current of 400-500 pA° and an accelerating voltage of 20 kV. All samples were screened for distinctive features before an automated particle analysis (software EDAX/AMETEK Genesis) was performed.

The chemical-mineral analyses were performed using electron probe microanalysis techniques (EPMA) with a JXA-8230 model JEOL superprobe at the Geoscience Institute of the University of Brasília in Brazil, under the supervision of Professor N. F. Botelho. The conditions applied to each analysis point were an accelerating voltage of 20 kV, a beam current of 40 nA°, a beam diameter of 1-2 μm and a counting time of 15 s for peak and 10 s for background. Specific standards were applied for the analysis of wolframite, cassiterite and micas.

The stable isotope ($\delta^{18}O$) study was carried out at the Isotope Geoscience Units of the Scottish Universities Environmental Research Centre Laboratories in Glasgow, Scotland, under the supervision of Professor A. E. Fallick. The nearly pure crystals samples were handpicked from selected specimens from the greisen. The oxygen isotope analyses were applied on cassiterite, wolframite, quartz and mica. Approximately 1 mg of oxygen bearing samples reacted with chlorine trifluoride (ClF_3) using laser heating fluorination techniques (Fallick *et al.* 1993, Macaulay *et al.* 2000). The precision of determinations from laboratory replicate analysis is 0.2‰ for $\delta^{18}O$ relative to Vienna Standard Mean Ocean Water (V-SMOW).

On the other hand, the sulfur isotope analyses ($\delta^{34}S$) were carried out at isotopic geology laboratories of the Geosciences Institute of the University of Brasília in Brazil, under the supervision of Professor B. M. Buhn (in memoriam). The nearly pure grain samples (chalcopyrite, pyrite,

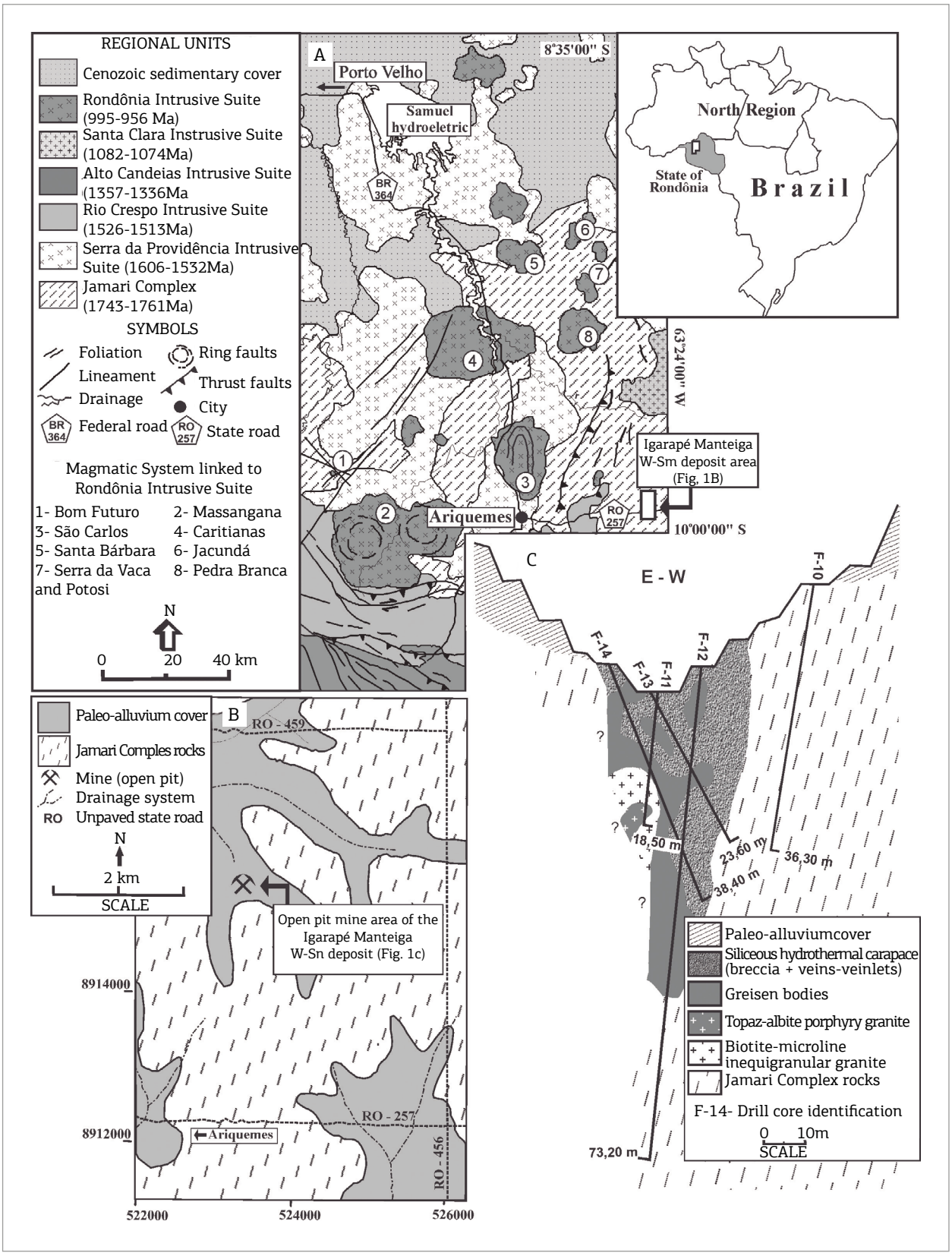

Figure 1. Location of the Rondônia Tin Province. (A) Regional geological map and location of the Igarapé Manteiga W-Sn deposit (modified from CPRM 2007); (B) Simplified geological map of the area around the Igarapé Manteiga W-Sn deposit (modified from Nascimento 2010); (C) Geological E-W cross section of the open pit mine area of the Igarapé Manteiga deposit. The vertical scale is exaggerated (compiled from METALMIG 2008).

sphalerite and molybdenite) were also handpicked from the selected veins. The grains were mounted in epoxy blocks and polished to obtain a smooth surface. The sulfur isotope content was obtained by means of laser ablation multiple-collector inductively coupled plasma mass spectrometry (LA-MC-ICP-MS), applied to each analysis point under an accelerating voltage of 20 kV, according to the analytical procedure described by Bender *et al.* (2007) and Silva *et al.* (2011). The calibration to the internal standards (NBS123, IAEA-S1 and IAEA-S2) yielded an analytical precision of around 0.4%.

The $^{40}Ar/^{39}Ar$ isotopic analyses on mica samples from greisen were carried out at the isotopic geology laboratories at Queen's University in the Department of Geological Sciences & Geological Engineering in Ontario (Canada), under the supervision of Professor D. A. Archibald. Mineral samples for $^{40}Ar/^{39}Ar$ analyses were obtained from hand samples that were ground by mortar and pestle, followed by a hand-picked selection that was placed under a binocular microscope to guarantee a high purity of mica flakes. ^{40}Ar-^{39}Ar isotopic analysis followed the analytical procedure described by Roddick (1983). The mineral concentrates were then irradiated for about 40 hours in a McMaster nuclear reactor. A specific 8 W Lexel 3500 ion laser (Ar), a MAP216 mass spectrometer with a Baur-Signer source and a multicollector electron were employed. Ages and errors were corrected using the formulas proposed by Steiger and Jäger (1977) and Dalrymple *et al.* (1981). The ^{40}Ar-^{39}Ar ages and errors shown represent an analytical precision of 2 σ or 0.5%, matching plateau variation form spectrum (McDougall & Harrison 1988). The ages obtained were referenced to the standard Hb3Gr (hornblende) from 1072 Ma (Roddick 1983).

REGIONAL GEOLOGICAL SETTING

The Paleoproterozoic basement in the north-central part of the Rondônia Tin Province is mainly represented by a regional unit called the Jamari Complex (Isotta *et al.* 1978). The Jamari Complex is formed by a variety of medium to high-grade gneisses of tonalitic-enderbitic or granodioritic-charnoenderbitic compositions, mafic orthogneisses, amphibolites and schist lenses. These rocks are polydeformed and present U-Pb crystallization ages between 1.76 and 1.67 Ga. However, they are marked by regional tectonometamorphic events from 1.67-1.63, 1.33 to 1.32 and 1.2 to 1.1 Ga. (Santos *et al.* 2000, 2008, Payolla *et al.* 2002, Tohver *et al.* 2005, Scandolara 2006, Souza *et al.* 2006, CPRM 2007, Bettencourt *et al.* 2010, Scandolara *et al.* 2013).

In this region, the Rondônia Tin Province comprises several Meso- to Neoproterozoic rapakivi granite suites (Fig. 1A), represented by the regional units called Serra da Providência (1606-1532 Ma), Rio Crespo (1526-1513 Ma), Alto Candeias (1357-1336 Ma), Santa Clara (1082-1074 Ma) and Rondônia (995-956 Ma) intrusive suites, respectively. In general, these granite suites are polyphasic stocks and batholiths with alkaline to subalkaline, metaluminous - peraluminous geochemical characteristics, and an A-type intraplate to post-collisional geochemical signature. They are locally deformed by shear zones (Souza *et al.* 1975, Leal *et al.* 1978, Bettencourt *et al.* 1999, 2006, 2010, CPRM 2007).

The Rondônia Intrusive Suite stands for having major mineralized sites in the region. This unit is composed of amphibole–biotite and alkali–feldspar syenogranites, syenites and microsyenites, and some rare rocks such as topaz-Li–mica albite and topaz-quartz-feldspar porphyry granites (Souza *et al.* 1975, Leal *et al.* 1978, Bettencourt *et al.* 1999, CPRM 2007). The primary mineralization (Sn, W, Nb, Ta) is linked to late- to post-magmatic hydrothermal phases, encapsulated in bodies of greisen, vein, breccia and pegmatite, associated with quartz, topaz, Li-F micas, fluorite, siderite, sphalerite, pyrite, chalcopyrite, arsenopyrite, galena, pyrrhotite, digenite-chalcocite, hematite, molybdenite, bismuthinite, monazite, thorite and others (Leite Jr. 2002, Souza 2003, Sparrenberger 2003, Bettencourt *et al.* 2005a, Nascimento 2010, Santos Jr. 2015). The available geochronological data on the timing of mineralization in the Rondônia Tin Province indicate that these late- to post-magmatic hydrothermal processes are very close to the ages of the late-stage rapakivi magmatic phases (Tab. 1). These data suggest that the metal-enriched hydrothermal phases were exsolved from the NYF (Nb>Y(REE)-F) affiliation magmatic phase during the final crystallization process (Lehmann 1982, Hedenquist & Lowenstern 1994, Burnham 1997, Černý & Ercit 2005, Richards 2011).

LOCAL GEOLOGICAL SETTING

The geological setting of the Igarapé Manteiga W-Sn deposit is formed by a granite stock intrusive in the Jamari Complex rocks (Fig. 1B). In general, these rocks show a thick weathering profile and are covered by an alluvium sequence. Underlying parent-rocks are only observed in the open-pit mine area or through drill core information (Figs 1C and 2A). Drill holes in the open-pit mine are mainly located on the apex zone of the granite stock. In this site, some drill core intercepted a magmatic system under the mineralized zones, which are formed by two granitic petrographic types: biotite-microcline granite and topaz-albite granite. W-Sn and other metals that are present were hosted in a hydrothermal carapace zone, encapsulated in greisen, breccia and vein-veinlets.

The Paleoproterozoic Jamari Complex is composed of ortho- and paragneiss, charnockites and amphibolite lenticular bodies. In general, these rocks exhibit medium to coarse grained texture, as well as a pronounced metamorphic foliation with a northeast-southwest trend and high (75°-85°) dips to the southeast. Often these rocks are crossed by fault and ductile shear zones with mylonitic texture generation (Nascimento 2010).

In the magmatic system, the biotite-microcline granite is pink in color, displays inequigranular medium- to coarse-grained texture and isotropic fabric. It is composed of microcline (35-38%), quartz (25-27%), plagioclase (An_{18-24}, 20-22%) and biotite (2-5%). The accessory minerals are zircon, apatite, fluorite, traces of monazite, pyrite and chalcopyrite. Chlorite, epidote, white mica and Fe-hydroxides are secondary minerals. On the other hand, the topaz-albite granite is light pink, displays inequigranular to porphyritic fine- to medium-grained texture and isotropic fabric. It is composed of quartz and microcline microperthitic anhedral and subhedral phenocrysts with grain sizes between 1.5 and 3.5 mm, embedded in a matrix formed by crystals aggregates with sizes ranging from 0.2 to 0.6 mm. Its essential minerals are microcline (15-18%), quartz (16-20%), plagioclase (albite = An_{4-6} 47-52%), topaz (8-12%) and mica (5-8%). Its accessory minerals are fluorite, carbonate, sphalerite, pyrite, chalcopyrite and traces of metamict zircon. Microcline and quartz phenocrysts contain frequent inclusions of albite laths arranged in a discontinuously rounded pattern. This textural feature is typically magmatic and is indicative of their crystallization from the late stage residual and highly fractionated granitic melts (Stemprok 1991, Schwartz 1992, Zhu *et al.* 2001, Lenharo *et al.* 2003).

The mineralized hydrothermal carapace zone presents an irregular contour distributed along the contacts between the cupola of the granite stock and the rocks of the Jamari Complex. It has an essentially siliceous to alumino-siliceous composition and brings together greisen, breccia and vein-veinlets. In this site, W-Sn and other metals are spread out or in massive clusters associated with gangue minerals (quartz, topaz, Li-micas, fluorite and others).

Finally, there is a thick alluvium sequence, categorized as a paleo-fluvial clastic deposit (Nascimento 2010), which completely covers the Igarapé Manteiga W-Sn deposit. This sedimentary cover is formed by a centimeter- to meter-scale stratal sequence, composed of laminated to trough laminae cycles of fine- to medium-grained conglomerates, sand

Table 1. Available geochronological data for the age of the mineralization in the Rondônia Tin Province.

Sn-W deposit	Regional unit	Method	Mineral	Rock type	Age (Ma)	References
Santa Bárbara	Rondônia Intrusive Suite (995-956 Ma)	Ar-Ar	zinnwaldite zinnwaldite zinnwaldite muscovite	syenogranite albite granite bedded greisen mica vein	990 ± 5 985 ± 4 959 ± 4 987 ± 1.9	Bettencourt *et al.* (2005b)
		K-Ar	zinnwaldite	greisen	961± 17	Leite Jr. *et al.* (2001)
Bom Futuro		Ar-Ar	zinnwaldite zinnwaldite	pegmatite quartz vein	994 ± 3 993 ± 3	Bettencourt *et al.* (2005b)
		K-Ar	zinnwaldite	quartz vein	969 ± 27	Leite Jr. *et al.* (2001)
		U-Th-Pb	monazite	greisen	997 ± 48	Souza *et al.* (2005)
Igarapé Manteiga		Ar-Ar	zinnwaldite	mica greisen	988 ± 5	This paper
Oriente Novo	Santa Clara Intrusive Suite (1082-1074 Ma)	K-Ar	zinnwaldite zinnwaldite zinnwaldite	greisen greisen quartz vein	1006 ± 17 981 ± 35 993 ± 16	Leite Jr. *et al.* (2001)
Rio Branco			zinnwaldite	greisen	976 ± 30	
Potosi		Ar-Ar	muscovite	mica greisen	1053 ± 3	Bettencourt *et al.* (2005b)
Oriente Novo		K-Ar	biotite	greisen	993 ± 40	Priem *et al.* (1971)
Liberdade	São Lourenço-Caripunas Intrusive Suite (1314-1309 Ma)	Ar-Ar	muscovite	mica greisen	1308 ± 5	Santos Jr. (2015)

and clay, and constitutes part of a channel fill. Important wolframite and cassiterite concentrations in coarse-grained aggregates occur associated to basal conglomerates.

HYDROTHERMAL ZONE

At this site, pervasive greisen alterations are dominant, followed by breccia and vein-veinlets. Greisen has truncates and irregular or intercalated geological contacts with breccia bodies, while the vein-veinlets crosses all rock types (Paleoproterozoic basement, cupola granitic, greisen and breccia) in a complex and multiple arrangement. Below we present the main features and the mineralogical composition of these hydrothermalized facies.

Greisen

Greisens are light green to light gray in color and have inequigranular medium- to coarse-grained texture and isotropic fabric (Fig. 2B). They are essentially composed of quartz, topaz, flourite, fengite and Li-mica in different proportions. Accessory minerals include wolframite, cassiterite, siderite, monazite, xenotime, hematite, chalcopyrite, sphalerite, pyrite, pyrrhotite, galena, bismuthinite and molybdenite. Additionally, Pereira *et al.* (2008) still reported the presence of some sulfides and exotic Ag- and Bi-telluride minerals (*e.g.* cervelleite = Ag_4TeS).

On the basis of Kühne et al. (1972, in Stemprok 1987) mineralogical quantitative classification proposed for greisen, we identified four exogreisen petrographic types: mica-topaz-quartz greisen, the dominant type, followed by topaz-mica-quartz greisen, quartz-topaz-mica greisen and, rarely, quartz-mica greisen (Fig. 2C). However, the contact relationships between these greisen varieties are not clear due to lack of exposure.

The essential mineral assemblage consists of euhedral to anhedral crystal aggregates, with grain sizes between 0.5 and 6 mm in inequigranular microtexture. Quartz and topaz aggregates are dominant and representative for the youngest minerals in the crystallization sequence of the studied greisens. The mica crystal aggregates are euhedral to subhedral, display grain sizes between 1 and 10 mm and pale-brown to orange-greenish pleochroism (Fig. 2D). Frequently, mica aggregates occur in a lamellar radiating manner associated with siderite anhedral and fengite aggregates. Flourite occurs as isolated subhedral crystals with grain sizes varying from 1 to 4 mm or in small interstitial aggregates (size < 1 mm) and disseminated in the quartz-topaz-mica assemblage.

The wolframite and cassiterite euhedral to subhedral crystals are spread out or occur in small aggregates, normally filling cavities associated with the essential mineralogy of greisens (Fig. 2E). They show grain size in a large range from 1 to about 30 mm and frequently display micro-fractures filled by chalcopyrite, pyrite and galena. However, occasionally wolframite ± cassiterite may occur as anomalous euhedral centimetric aggregate crystals (Fig. 2F).

Vein-Veinlets

These represent a complex and interlaced set of subvertical tensile fractures/fissures crossing greisen and breccia and extend to the basement rocks from within the granitic cupola. They present varied thicknesses, inequigranular medium- to coarse-grained textures and isotropic fabrics, and are essentially composed of quartz-topaz-mica aggregates, but may contain fluorite, siderite, hematite, ore- and sulfide-minerals. Frequently, vein-veinlets display successive asymmetrical crustification, marked by growth of quartz, topaz and mica crystals from fissure walls towards the center, forming a comb structure (Figs. 3A and 3B). Occasionally, in the central part of some thicker veins, dilated zones or sheeted cavities occur, which are partially to totally filled by ore- and sulfide-minerals associated with euhedral Li-micas (Fig. 3C).

According to Jensen and Bateman (1981), the reopening processes of the fissures, which permits further deposition, generally causes successive crustification. On the other hand, the cavity filling involves two separate processes: dilatation/opening and deposition of the minerals. The two may operate almost simultaneously, but normally they are independent processes that are separated by an interval of time. These features are diagnostic of an effective and protracted hydrothermal re-circulation convective process.

The continuing hydrothermal supplies that go into fissures or cavities may lead to metasomatic replacement, by which new minerals replace earlier formed minerals. This process may lead to partial or total filling of openings, which consequently causes the fluid flow to be significantly constrained. This increases the confined fluid pressure (*i.e.* reservoir of hydrothermal solutions) and favors subsequent hydraulic fracturing from the forceful fluidal with the generation of new veins that cross the earlier veins (Phillips 1972, Guha *et al.* 1983, Foxford *et al.* 2000, Liu *et al.* 2015).

Breccia

The breccia bodies studied are essentially monomictic, but can be locally polymictic and are formed by a highly variable large-fragment size (between 2 and 25 cm), which are mainly distributed in a fragment-supported textural arrangement containing more than 80% fragments (Fig. 3D). The fragments are typically angular and formed predominantly of quartz (products from fragmentation of siliceous hydrothermal carapace and vein), but occasional fragments of greisen and basement rocks also occur, as well

as fragments of ore minerals (wolframite and cassiterite) and some sulfide mineral (pyrite, chalcopyrite, galena). These fragments are immersed in a matrix composed by essential mineralogy from greisen. The interfragmental space is completely filled by quartz, topaz, Li-mica, fluorite and siderite aggregates in various proportions, as well as hematite, goethite, ore- and sulfide minerals. Occasionally, in the matrix, irregular vugs occur, which are partially filled by quartz-fluorite-mica and encrustational growth of pyrite. In general, the fabric is typically fragment-supported, but locally occurs as matrix-supported, especially in the Li-mica rich portions.

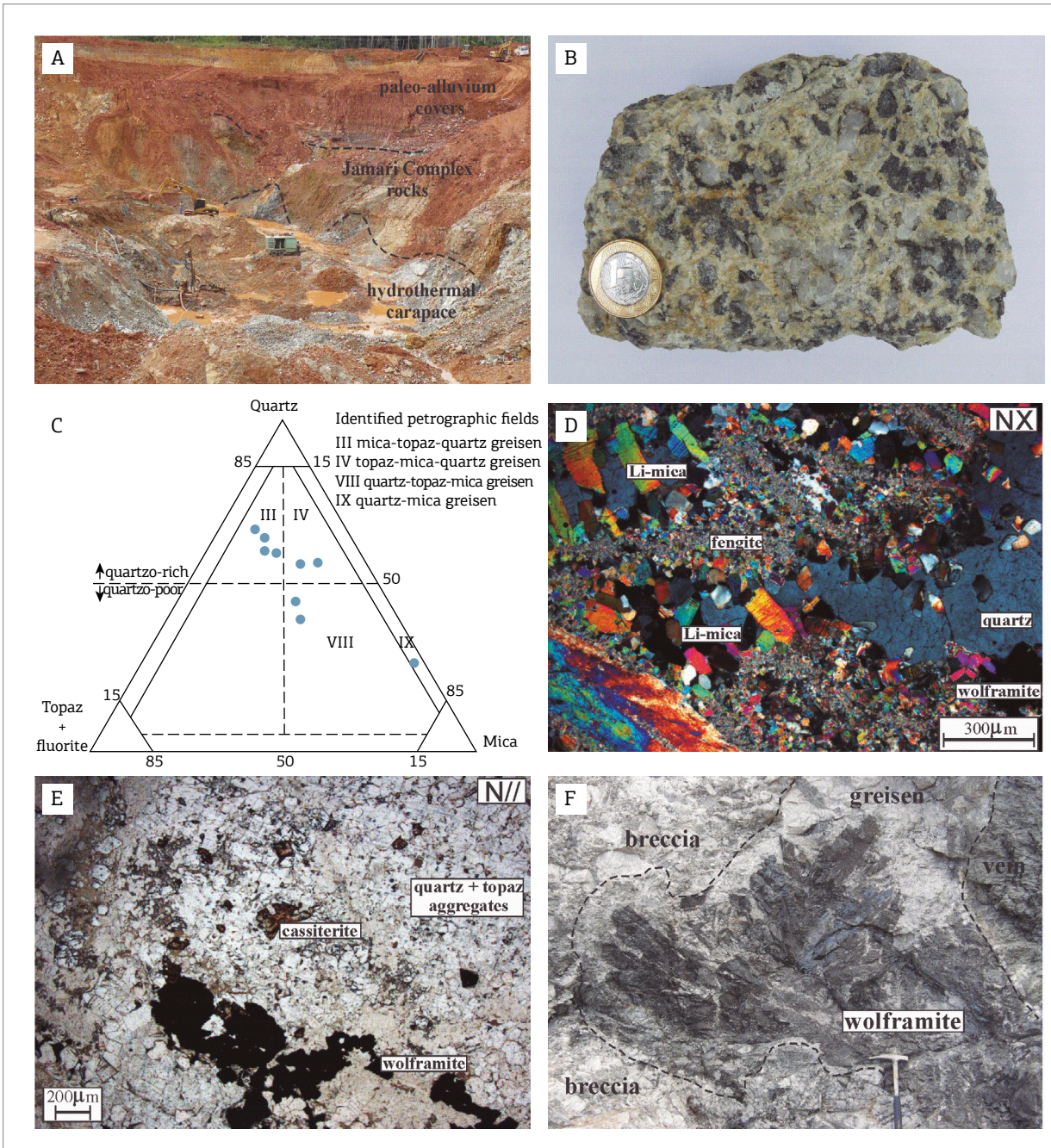

Figure 2. (A) Open-pit mine area developed in the apex-zone of the Igarapé Manteiga granitic stock; (B) Macroscopic textural arrangement of the mica-topaz-quartz greisen; (C) Quantitative classification of the Igarapé Manteiga greisen, applying the diagram proposed by Kühne *et al.* (1972, in Stemprok 1987); (D) Microtexture of topaz-mica-quartz greisen (NX = crossed nicols); (E) Microtexture of quartz-topaz-mica greisen with wolframite and cassiterite disseminated crystals (N// = parallel nicols); (F) Wolframite large crystals developed in greisen. Observe the truncate and irregular geological contacts of the breccia and vein.

Based on the studies of Laznicka (1989) and Jébrak (1997), these breccia bodies can be classified as hydrothermal, and originate from effective fluidal pressure beneath a siliceous to alumino-siliceous hydrothermal carapace that led to fracture propagation, corrosive wear and hydraulic fragmentation. The field observations suggest that this fragmentation process was cyclical and formed successive breccia bodies. According to Plimer (1987), the hydraulic fragmentation process can be repeated many times, resulting in an extended sequence of breccia bodies and sheeted vein systems.

MINERALOGY

In this section, we present the petrographic features and chemical data on the sulfide mineral assemblage, ore-minerals (wolframite and cassiterite) and mica. This information helps to understand the mineral substitution mechanisms and the zoning patterns in a hydrothermal environment. Additionally, the chemical study on mica from greisen aims to support discussions of ^{40}Ar-^{39}Ar geochronological analysis.

Sulfide mineral assemblage

The sulfide mineral assemblage in the greisen and veins showed petrographic texture diagnostics for a paragenetic sequence formation, which is probably linked to lowering temperature and physico-chemical changes (pressure, pH and Eh conditions) in the hydrothermal environment.

Sphalerite and pyrrhotite in anhedral to subhedral crystals have grain sizes between 30 and 90 μm, exhibit corroded borders, probably because of mineral-fluid interaction, as well as micro-inclusions of chalcopyrite, pyrite (I) and galena, mainly filling micro-fractures (Fig. 4A). Sphalerite and pyrrhotite represent the earliest sulfide-mineral phase at a high temperature (300-350°C) within hydrothermal environments exsolved from cooling and crystallizing granitic magmas (Yund & Hall 1969, Stanton 1972, Ohmoto & Rye 1979, Barton & Skinner 1979).

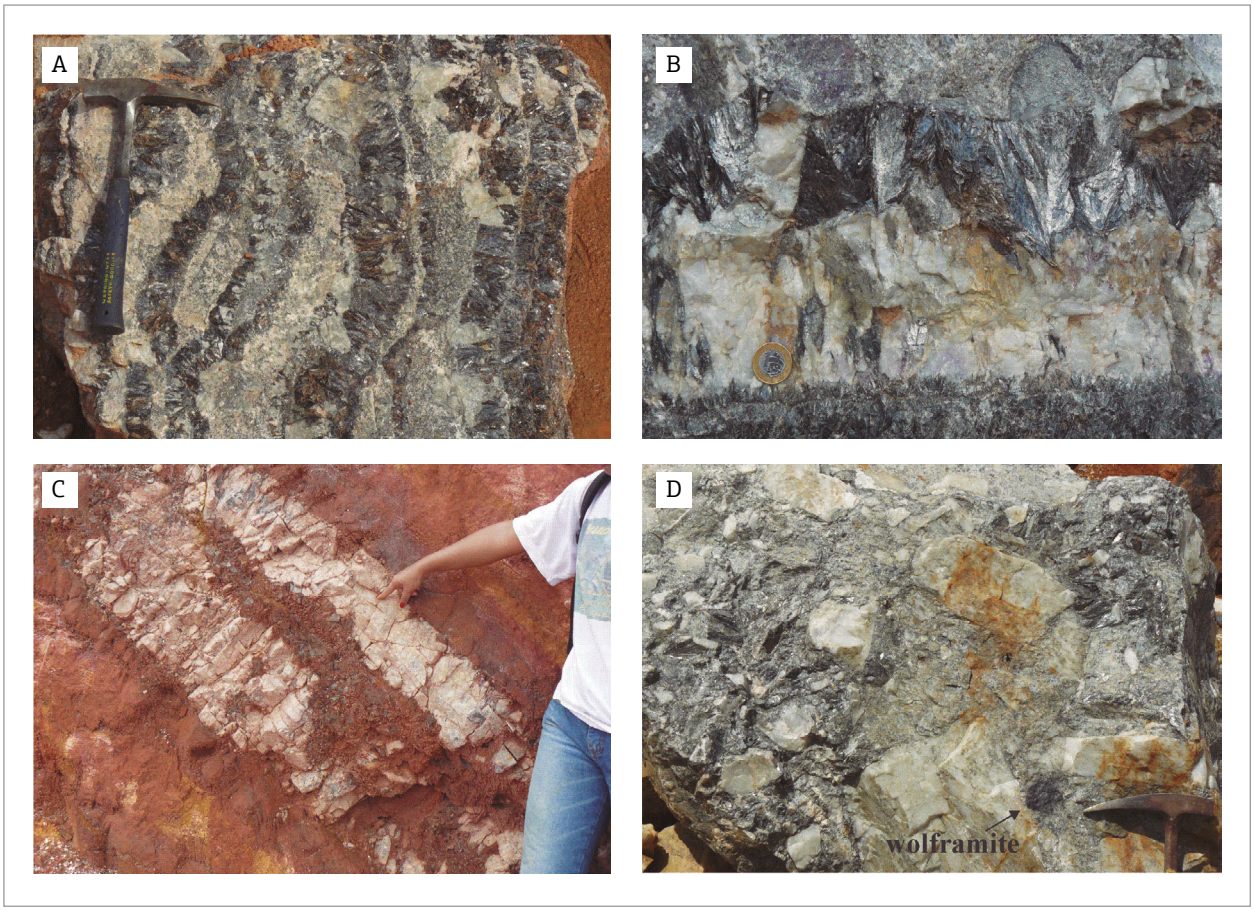

Figure 3. (A) Asymmetrical crustification texture in veins, with crusts of Li-micas, quartz and topaz, with some contributions of fluorite, siderite, ore- and sulfide minerals; (B) Comb structure in veins, mainly formed by growth quartz, topaz and mica crystals from fissure walls towards the center; (C); Thicker vein with central part filled by ore- and sulfide minerals associated to euhedral Li-micas aggregates; (D) Macroscopic textural arrangement of the polymictic breccia containing ore-mineral (wolframite) fragments.

The interstices between pyrrhotite and sphalerite crystals are frequently occupied by the subsequent sulfide-mineral phase, probably at a moderate temperature (300-250°C), formed by chalcopyrite, pyrite (I) and galena anhedric aggregates (Ohmoto & Lasaga 1982, Vaughan & Craig 1997).

Sometimes, there are pyrrhotite crystals with corroded borders that are partially replaced by pyrite (II) anhedral and subhedral aggregates. Generally, this replacement reaction involves the dissolution of the pyrrhotite immediately followed by the precipitation of the pyrite (Murowchic 1992,

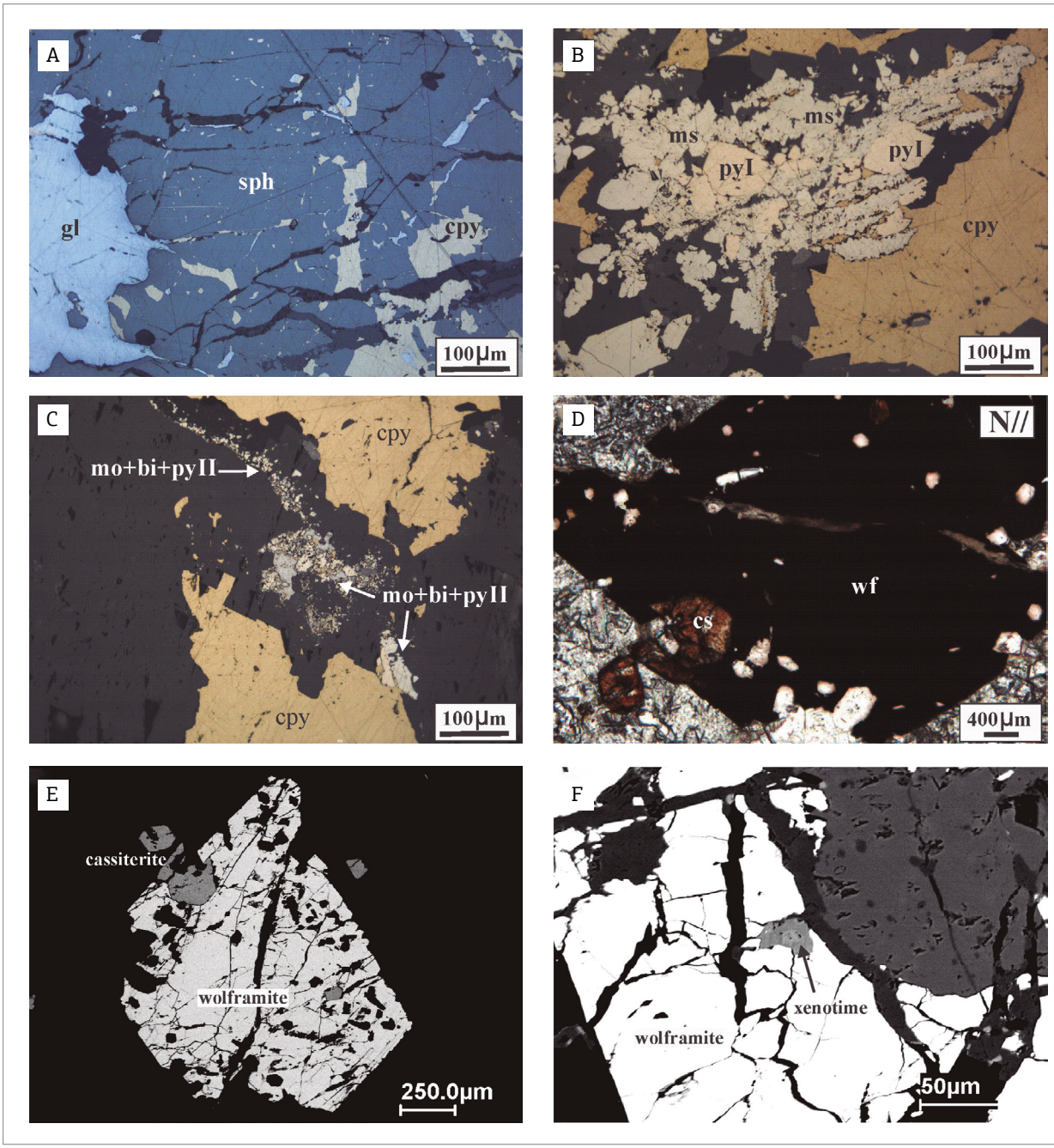

Figure 4. Photomicrograph of sulfide-mineral and wolframite-cassiterite assemblage. (A) Chalcopyrite and galena occupying interstices or filling micro-fractures in sphalerite; (B) isometric pyrite (I) partially replaced by orthorhombic marcasite; (C) Bismuthinite, molybdenite and pyrite II aggregates forming fillets encrusted on the borders of preterit sulfide-minerals and filling fissures; (D) Wolframite-cassiterite aggregate in mica-topaz-quartz greisen (N// = parallel nicols); (E) BSE image of wolframite-cassiterite aggregate; (F) BSE image of xenotime micro-inclusion in wolframite. The symbols are bi = bismuthinite, cpy = chalcopyrite, gl = galena, mo = molybdenite, mr = marcasite, py = pyrite, sph = sphalerite, cs = cassiterite and wf = wolframite.

Vaughan & Craig 1997, Qian *et al.* 2011). The monoclinic pyrrothite ± pyrite association, under a hydrothermal environment, is stable between 220 and 250°C (Stanton 1972, Kissin & Scott 1982, Qian *et al.* 2011, Chareev *et al.* 2014). Additionally, isometric pyrite (I) is partially replaced by orthorhombic marcasite (Fig. 4B). This is a polymorphic replacement that occurs mainly due to the lowering of the temperature and under delicate physico-chemical conditions (*i.e.* pH < 5, T ≤ 250°C), as well as from effective actions of the H_2S_2-hydrothermal solution (Murowchick & Barnes 1986, Murowchick 1992).

Finally, the last sulfide-mineral phase recognized is composed of a bismuthinite, molybdenite and pyrite II assemblage. Generally, these minerals have euhedral to subhedral shapes, measure less than 30 μm and occur in interstices between grains or forming fillets encrusted on the borders of preterit sulfide-minerals, as well as filling micro-fissures (Fig. 4C). However, studies are contradictory about the temperature of bismuthinite and molybdenite solubility and precipitation under hydrothermal conditions (Wood & Samson 1998, Seward & Branes 1997). The mode of occurrence (interstitial or in fillets encrusted), as well as the presence of Ag-sulfides and tellurides, can be indicative of low temperature (T < 250°C) conditions (Wood *et al.* 1987, Vaughan & Craig 1997, Seward & Branes 1997). Additionally, the presence of pyrite (II) euhedral crystals may also indicate the action of successive S-supply or an excess of sulfur consumption present in the lower temperature residual hydrothermal solution (Vaughan & Craig 1997, Seward & Barnes 1997).

Wolframite

The opaque crystals of wolframite normally occur in association with cassiterite crystals. They are fractured and apparently clean (Figs. 4D and 4E). However, electron microscopy investigations reveal the presence of some micro-inclusions of monazite, xenotime and Nb-Ta-Fe oxide minerals (Fig. 4F).

Wolframite [(Fe, Mn)WO_4] is the intermediate member of a complete solid-solution, which has ferberite ($FeWO_4$) and hübnerite ($MnWO_4$) as end members (Hsu 1976, Waychunas 1991). The microprobe analyses on the wolframite crystals show a tendency of ferberite, whose FeO (total) content is about two times greater than the MnO content, while the Nb_2O_5 + Ta_2O_5 content is around 1 wt.% (Tab. 2). In the W *vs* Fe *vs* Mn atomic concentrations triangular diagram, the tendency is also observed of analytical results moving to the iron vertex (Fig. 5A). In general, the analytical results point to a chemical structural formula that can be expressed as $(Fe_{0.61\text{-}0.71}\ Mn_{0.32\text{-}0.42})WO_4$. These results are also consistent with the data available for the Bom Futuro tin deposit in the Rondônia Tin Province (Souza & Botelho 2009).

The wolframite crystals show some Nb and Ta impurities, most likely resulting from coupled substitution, according to the following equation: $Fe^{2+} + W^{6+} \leftrightarrow Fe^{3+} + (Nb,Ta)^{5+}$ (Polya 1988). This substitution may be favored by a relative decrease in W^{6+} in conjunction with the increase in Nb^{5+} + Ta^{5+} (Fig. 5B), with the electrostatic charge deficiency resulting from this substitution being compensated by the oxidation from Fe^{2+} to F^{3+}, as diagnosed by the diagram of atomic correlation Fe^{3+}calc. *vs* Nb^{5+} + Ta^{5+} (Fig. 5C). Due to the low content of Ta (Tab. 2), this element probably joint Nb as a participate in a coupled substitution (Neiva 2008). Wolframite analyses have the highest calculated Fe^{2+} values (Tab. 2), which suggests that they precipitated from reduced hydrothermal fluids.

According to Hsu (1976) and Ivanova (1988), the ferberite member is stable under oxidizing conditions and temperatures above 400°C. Therefore, it is possible that the Nb-Ta-Fe oxide minerals included in wolframite are exsolution generated during the lowering of the temperature.

Cassiterite

The crystals of cassiterite exhibit irregular and discontinuous growth-zones, whose colors range from light-yellow to dark-orange (Fig. 4D). They contain between 91.18-98.25 wt.% SnO_2, 0.30-2.52 wt.% FeO_{total}, 0-1 wt.% Nb_2O_3, 0-4 wt.% Ta_2O_3, and very low concentrations of Ti, W, Mn and U impurities (Tab. 2). The Ta_2O_3 contents can be considered relatively high for cassiterite, which is usually below 2 wt.% (Neiva 1996, 2008, Souza & Botelho 2009, Costi *et al.* 2000). The light-yellow growth-zones are nearly pure SnO_2, whereas the dark-orange ones have some $FeO_{(total)}$, TiO_2, Ta_2O_5, Nb_2O_5 and WO_3 contents. These results in general are also consistent with the data available for the Bom Futuro tin deposit in the Rondônia Tin Province (Souza & Botelho 2009), as well as for other tin deposits (Giuliani 1987, Murciego *et al.* 1997).

The variations in cassiterite composition have been discussed by several authors (Neiva 1996, 2008, Murciego *et al.* 1997, Möller *et al.* 1998). According to these authors, the main mechanisms are replacements of Sn by Fe + Ti impurities, attributed to the change in composition of hydrothermal fluids with decreasing temperature, and controlled by the Equations 1 and 2:

$$2Sn^{4+} + O^{2+} \leftrightarrow Ti^{4+} + Fe^{3+} + OH^- \quad (1)$$

$$3(Sn, Ti)^{4+} \leftrightarrow 2(Nb,Ta)^{5+} + Fe^{2+} \quad (2)$$

The analyses on the cassiterite crystals presented these replacement types, illustrated by the negative atomic correlation diagrams Sn *vs* Fe + Ti and Sn *vs* Nb+Ta (Figs. 6A

Table 2. Electron microprobe data on the chemical composition of the wolframite and cassiterite. Oxides in wt.% and element in atoms per formula unit (apfu). Cation formula calculated on four atoms of oxygen for wolframite and on two atoms of oxygen for cassiterite.

wolframite												
Spots	1	2	3	4	5	6	7	8	9	10	11	12
WO_3	75.04	73.97	73.95	74.88	74.71	74.57	74.36	75.40	74.99	75.80	75.79	76.14
SnO_2	0.00	0.00	0.00	0.00	0.00	0.00	0.00	0.01	0.00	0.00	0.00	0.00
TiO_2	0.00	0.03	0.00	0.01	0.00	0.00	0.00	0.06	0.01	0.00	0.01	0.02
CaO	0.01	0.00	0.02	0.01	0.00	0.00	0.27	0.02	0.00	0.00	0.00	0.02
Nb_2O_3	0.73	0.54	0.75	0.74	0.96	0.61	1.01	0.81	0.59	0.68	0.76	0.51
Ta_2O_3	0.36	0.20	0.36	0.38	0.40	0.31	0.17	0.22	0.20	0.23	0.18	0.18
$FeO_{(tot.)}$	15.61	16.77	15.51	15.64	16.23	14.53	15.73	15.65	15.51	15.62	15.17	15.18
MnO	9.11	7.57	9.07	8.95	8.40	9.87	8.76	8.80	8.89	8.85	8.87	8.99
Total (wt.%)	100.86	99.08	99.66	100.61	100.70	99.89	100.30	100.97	100.19	101.18	100.78	101.04
W	0.970	0.974	0.967	0.970	0.966	0.974	0.964	0.973	0.976	0.977	0.980	0.983
Sn	0.000	0.000	0.000	0.000	0.000	0.000	0.000	0.000	0.000	0.000	0.000	0.000
Ti	0.000	0.001	0.000	0.001	0.000	0.000	0.000	0.002	0.001	0.000	0.001	0.001
Ca	0.001	0.000	0.001	0.001	0.000	0.000	0.015	0.001	0.000	0.000	0.000	0.001
Nb	0.016	0.012	0.017	0.017	0.022	0.014	0.023	0.018	0.013	0.015	0.017	0.012
Ta	0.005	0.003	0.005	0.005	0.005	0.004	0.002	0.003	0.003	0.003	0.003	0.003
Fe^{2+}calc.	0.621	0.686	0.622	0.624	0.644	0.586	0.622	0.624	0.628	0.627	0.614	0.616
Fe^{3+}calc.	0.030	0.026	0.033	0.030	0.034	0.026	0.036	0.027	0.024	0.023	0.020	0.017
Mn	0.385	0.326	0.388	0.379	0.355	0.421	0.371	0.371	0.378	0.373	0.375	0.380
Total (apfu)	2.028	2.028	2.033	2.027	2.026	2.025	2.033	2.019	2.023	2.018	2.010	2.012
wolframite												
Spots	13	14	15	16	17	18	19	20	21	22	23	
WO_3	75.81	76.09	75.79	75.80	75.42	75.98	75.68	75.63	75.07	75.35	75.56	
SnO_2	0.00	0.00	0.00	0.00	0.00	0.00	0.00	0.00	0.00	0.00	0.00	
TiO_2	0.00	0.01	0.00	0.00	0.02	0.00	0.00	0.01	0.00	0.01	0.00	
CaO	0.02	0.01	0.00	0.00	0.02	0.00	0.00	0.00	0.00	0.00	0.00	
Nb_2O_3	0.71	0.72	0.74	0.76	0.83	0.77	0.70	0.78	0.60	0.82	0.70	
Ta_2O_3	0.33	0.27	0.26	0.24	0.21	0.22	0.27	0.23	0.28	0.38	0.25	
$FeO_{(tot.)}$	15.51	15.22	15.34	15.30	15.21	15.40	15.37	15.36	15.58	15.27	15.45	
MnO	8.92	8.83	9.06	9.08	8.91	8.94	9.03	9.00	8.95	8.89	9.11	
Total (wt.%)	101.30	101.15	101.19	101.18	100.60	101.31	101.05	101.01	100.48	100.72	101.07	
W	0.975	0.981	0.977	0.977	0.977	0.978	0.976	0.976	0.974	0.975	0.975	
Sn	0.000	0.000	0.000	0.000	0.000	0.000	0.000	0.000	0.000	0.000	0.000	
Ti	0.000	0.001	0.000	0.000	0.001	0.000	0.001	0.000	0.000	0.000	0.000	
Ca	0.001	0.001	0.000	0.000	0.001	0.000	0.000	0.000	0.000	0.001	0.000	
Nb	0.016	0.016	0.017	0.017	0.019	0.017	0.016	0.018	0.014	0.019	0.016	
Ta	0.005	0.004	0.004	0.003	0.003	0.003	0.004	0.003	0.004	0.005	0.003	
Fe^{2+}calc.	0.618	0.614	0.614	0.613	0.612	0.617	0.616	0.616	0.627	0.613	0.618	
Fe^{3+}calc.	0.025	0.019	0.023	0.023	0.023	0.022	0.024	0.024	0.026	0.025	0.025	
Mn	0.379	0.372	0.382	0.383	0.377	0.376	0.381	0.380	0.380	0.376	0.384	
Total (apfu)	2.019	2.008	2.017	2.016	2.013	2.013	2.018	2.017	2.025	2.014	2.021	

Continue...

Table 2. Continuation.

cassiterite												
Spots	1	2	3	4	5	6	7	8	9	10	11	12
SnO_2	91.18	91.28	90.85	91.61	92.53	91.20	92.57	92.67	94.24	93.72	94.49	95.30
TiO_2	0.24	0.39	0.50	0.63	0.66	0.53	0.73	0.40	0.38	0.65	0.62	0.76
Nb_2O_5	2.09	0.99	1.02	0.75	0.87	0.97	0.87	0.93	0.74	0.60	0.59	0.33
Ta_2O_5	1.70	4.50	4.27	3.73	3.63	4.32	3.41	3.47	2.92	2.48	2.30	1.38
$FeO_{(tot.)}$	2.52	1.43	1.38	1.27	1.11	1.20	1.07	1.08	0.89	1.00	1.07	0.66
WO_3	1.25	0.25	0.28	0.87	0.29	0.24	0.16	0.14	0.08	0.42	0.62	0.68
MnO	0.21	0.01	0.07	0.09	0.06	0.02	0.04	0.00	0.00	0.02	0.13	0.05
UO_2	0.00	0.03	0.00	0.03	0.00	0.00	0.00	0.00	0.00	0.00	0.00	0.00
Total (mol%)	99.19	98.88	98.37	98.98	99.15	98.48	98.85	98.69	99.25	98.89	99.82	99.16
Sn	0.911	0.922	0.920	0.929	0.929	0.923	0.931	0.937	0.947	0.943	0.942	0.955
Ti	0.005	0.007	0.010	0.012	0.012	0.010	0.014	0.007	0.007	0.012	0.012	0.014
Nb	0.024	0.011	0.012	0.009	0.010	0.011	0.010	0.011	0.008	0.007	0.007	0.004
Ta	0.012	0.031	0.030	0.026	0.025	0.030	0.023	0.024	0.020	0.017	0.016	0.009
Fe	0.053	0.030	0.030	0.027	0.023	0.025	0.023	0.023	0.019	0.021	0.022	0.014
W	0.008	0.002	0.002	0.001	0.002	0.002	0.001	0.001	0.001	0.003	0.004	0.004
Mn	0.004	0.000	0.002	0.002	0.001	0.001	0.001	0.000	0.000	0.000	0.003	0.001
U	0.000	0.001	0.000	0.001	0.000	0.000	0.000	0.000	0.000	0.000	0.000	0.000
Total (apfu)	1.017	1.004	1.006	1.007	1.003	1.002	1.003	1.002	1.002	1.003	1.006	1.001

cassiterite											
Spots	13	14	15	16	17	18	19	20	21	22	23
SnO_2	95.97	95.13	95.48	95.48	98.25	98.14	97.94	97.73	95.36	97.93	97.46
TiO_2	0.70	1.23	1.23	0.80	0.12	0.16	0.05	0.11	0.49	0.05	0.07
Nb_2O_5	0.29	0.27	0.27	0.40	0.03	0.00	0.04	0.13	0.41	0.01	0.41
Ta_2O_5	1.38	1.11	1.08	1.36	0.07	0.04	0.03	0.23	1.52	0.01	0.12
$FeO_{(tot.)}$	0.55	0.63	0.68	0.86	0.30	0.26	0.32	0.41	0.77	0.44	0.42
WO_3	0.20	0.43	0.40	0.08	0.00	0.00	0.00	0.02	0.70	0.60	1.12
MnO	0.00	0.03	0.00	0.03	0.06	0.03	0.01	0.00	0.16	0.06	0.09
UO_2	0.00	0.00	0.00	0.00	0.00	0.00	0.00	0.00	0.01	0.00	0.02
Total (mol%)	99.09	98.83	99.14	99.01	98.83	98.63	98.39	98.63	99.42	99.10	99.69
Sn	0.963	0.952	0.953	0.957	0.993	0.993	0.994	0.989	0.955	0.988	0.975
Ti	0.013	0.023	0.023	0.015	0.002	0.003	0.001	0.002	0.009	0.001	0.001
Nb	0.003	0.003	0.003	0.005	0.000	0.000	0.000	0.001	0.005	0.000	0.005
Ta	0.009	0.008	0.007	0.009	0.001	0.000	0.000	0.002	0.010	0.000	0.001
Fe	0.012	0.013	0.014	0.018	0.006	0.006	0.007	0.009	0.016	0.009	0.009
W	0.001	0.003	0.003	0.001	0.000	0.000	0.000	0.000	0.005	0.004	0.007
Mn	0.000	0.001	0.000	0.001	0.001	0.001	0.000	0.000	0.003	0.001	0.002
U	0.000	0.000	0.000	0.000	0.000	0.000	0.000	0.000	0.000	0.000	0.000
Total (apfu)	1.001	1.003	1.003	1.006	1.003	1.003	1.002	1.003	1.003	1.003	1.000

and 6B). Additionally, the W+Mn+Ti contents vary in proportion to the Fe contents (Fig. 6C), providing for the formation of a molecular wolframite species in the darker growth-zones, controlled by a type of coupled replacement, which can be described by Equation 3:

$$2(Sn, Ti)^{4+} \leftrightarrow (W, Mn)^{6+} + Fe^{2+} \quad (3)$$

This can be illustrated by the negative atomic correlation diagram Sn+Ti *vs* Fe+W+Mn (Fig. 6D).

These data indicate that Equations (2) and (3) controlled the substitution mechanisms for Nb+Ta and W+Mn impurities in crystals of cassiterite, which are linked to Fe/Ti ratios in dark-orange growth-zones. This is strongly supported when the compositions of cassiterite crystals are plotted in the (Nb,Ta) *vs* (Fe, W, Mn) *vs* (Sn, Ti) apfu triangular composition diagram (Fig. 7). They tend to align approximately along the (Sn,Ti) – (Fe,W,Mn)(Nb,Ta) joint, indicating that the $3(Sn, Ti)^{4+} \leftrightarrow 2(Nb,Ta)^{5+} + (Fe,W,Mn)^{2+}$ substitution mechanism is dominant. On the other hand, Equation (1) controlled the coupled substitution mechanisms of Sn by Fe+Ti in light-yellow growth-zones, which would have been responsible for the change in color of the cassiterite.

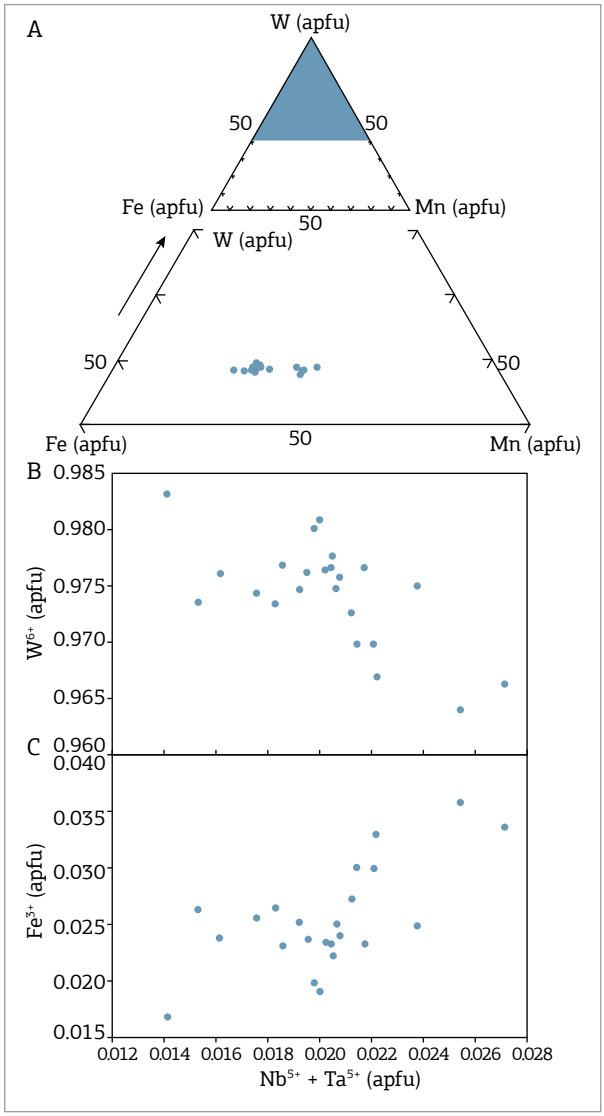

Figure 5. Atomic correlation diagrams (apfu) applied to wolframite crystals. (A) W *vs* Fe *vs* Mn triangular diagram; (B) W^{6+} *vs* $Nb^{5+} + Ta^{5+}$; (C) Fe^{3+} *vs* $Nb^{5+} + Ta^{5+}$.

Mica

Normally the mica crystals exhibit a black to dark green color and occur as euhedral to subhedral book aggregates with wide variation sizes. In the greisen and breccia, the mica crystals have a size ranging from 1 to 10 mm, but in the dilated zone of some thicker veins, this size can reach around 5 cm and draw comb and radial arrangements. In general, in greisen petrography observations, the mica crystals display from yellowish-orange-green to bluish-light brown-purple pleochroism, show slightly undulous extinction, and contain some Ti-Fe-hydroxide mineral inclusions. U-Th mineral micro-inclusions are rarely observed in the development of pleochroic haloes.

The microprobe analyses of the mica crystals from quartz-topaz-mica greisen showed that they are trioctahedral sheets (Tab. 3), based on a nomenclature proposed by Rieder *et al.* (1998). They have LiO_2 = 3-4 wt.%, F = 5-6 wt.%, MgO < 3 wt.%, SiO_2 = 44-48 wt.%, Al_2O_3 = 24-26 wt.% and FeO = 6-11 wt.%. On the Li *vs* Al^{VI}+Ti *vs* $Fe_{tot.}$+Mn+Mg triangular diagram, the analyses plot on the zinnwaldite field, with a composition near the midpoint of the polylithionite-siderophylite joint (Fig. 8). In general, these micas have similar chemical compositions to the other Li-Fe zinnwaldite from greisen, which is linked to evolved granitic systems of the Rondônia Intrusive Suite (Lowell & Ahl 2000, Leite Jr. 2002, Souza 2003). According to Lowell and Ahl (2000), Li-Fe zinnwaldite from greisens and veins linked to evolved granitic systems from Rondônia were crystallized at temperatures around 500°C, with a pressure between 1-500 bar and fO_2 around 10^{-23}.

STABLE ISOTOPE

In this section, we present data from stable isotopes ($\delta^{18}O$ and $\delta^{34}S$) obtained in the ore-minerals (wolframite and cassiterite), quartz and sulfide-mineral assemblages from greisen and veins. These data can provide information on the environment and crystallization temperature for the hydrothermal mineral assemblage and mineralization.

Oxygen Isotope ($\delta^{18}O$)

The oxygen isotope studies were focused on the ore minerals and applied the wolframite + quartz and cassiterite + quartz pairs from greisen, which showed an apparent equilibrium in hydrothermal assemblage. The isotopic results have a degree of uncertainty of ± 0.2‰, which are in Table 4 and are discussed below.

Wolframite ($\delta^{18}O$ = 0.6-0.9‰), cassiterite ($\delta^{18}O$ = 1.6-1.8‰) and quartz ($\delta^{18}O$ = 9.1-9.7‰) have revealed subtle variations in the respective oxygen isotope compositions, which indicate relative isotopic equilibrium with a common fluid. The different $\delta^{18}O$ values for wolframite, cassiterite and quartz are indicative of isotopic fractionation during the rise of the hydrothermal fluid and consequent mineral crystallization. Low values of $\delta^{18}O$ (from 0‰ to 10‰) are recorded in many Sn-W hydrothermal deposits and are interpreted as a consequence of the mixing between isotopically light meteoric fluids and magmatic fluids (Kelly & Rye 1979, Higgins & Kerrich 1982, Campbell *et al.* 1984, Sun & Eadington 1987). However, because quartz is less sensitive to isotopic changes in the hydrothermal environment,

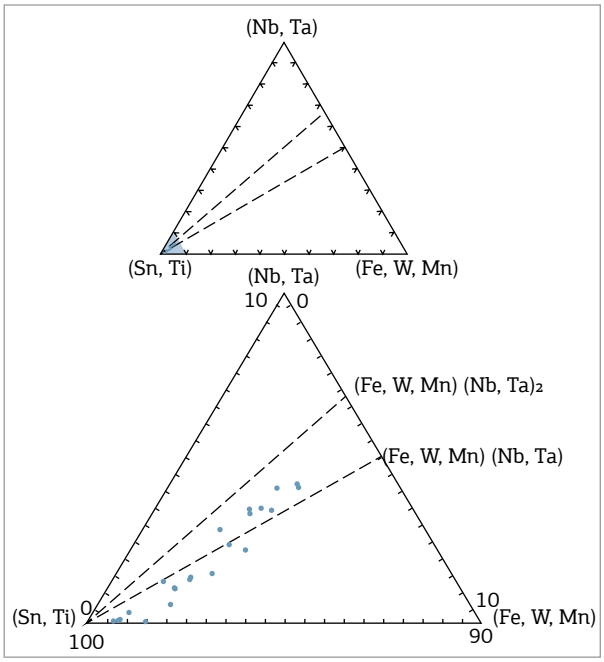

Figure 7. Composition triangular diagram plotted in terms of (Na,Ta)–(Fe,Mn)–(Sn,Ti) for cassiterite (Neiva 2008).

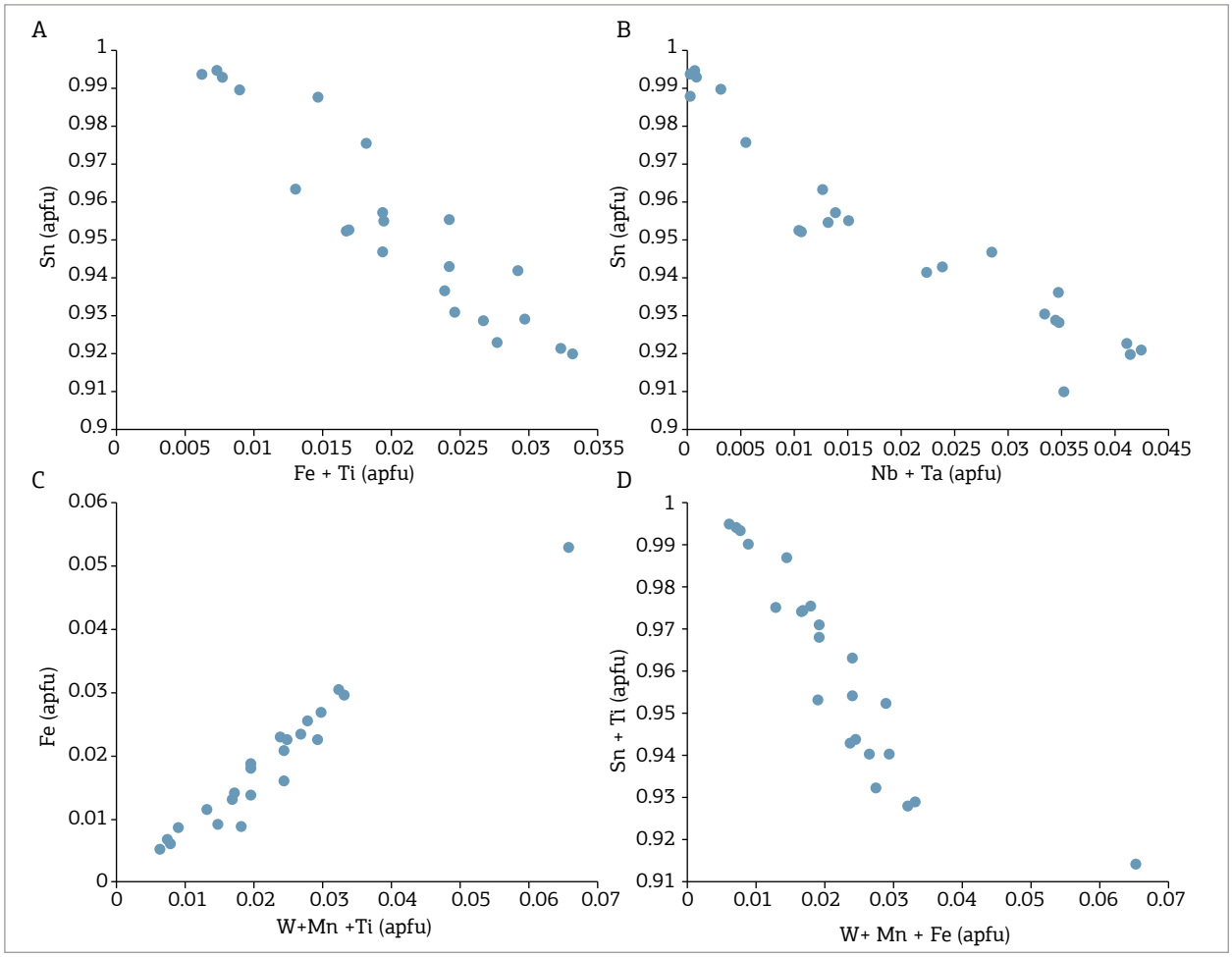

Figure 6. Atomic correlation diagrams applied to cassiterite crystals. (A) Sn *versus* Fe + Ti; (B) Sn *versus* Nb+Ta; (C) Fe *versus* W+Mn+ Ti; (D) Sn+ Ti *versus* W+Mn+Fe.

the $\delta^{18}O$ composition in the range of 9.1 to 9.7 ‰ is consistent with an isotopic signature for magmatic fluids (Taylor Jr. 1974, 1978).

The use of an $\delta^{18}O$ composition in isotopically equilibrated mineral pairs can also be applied as a geothermometer (Taylor Jr. 1997, Alderton 1989, Zheng 1992, Zhang *et al.* 1994). From this perspective, we used wolframite-quartz and cassiterite-quartz pairs to calculate the temperatures of the W-Sn mineralization in greisen. These calculations were based on two fractionation equations:

Table 3. Electron microprobe data on the chemical composition of the Li-Fe zinnwaldite. Li_2O and H_2O calculations after Tindle and Webb (1990).

Spots	1	2	3	4	5	6	7	8	9	10	11	12
SiO_2	46.33	44.14	46.96	46.75	47.66	46.36	46.77	47.74	47.29	47.69	47.92	46.53
TiO_2	0.11	-	0.19	0.08	0.10	0.07	0.09	-	0.26	-	0.40	0.33
Al_2O_3	23.91	24.78	25.51	25.24	26.10	25.10	24.39	25.00	25.06	25.18	25.54	25.69
FeO	11.08	9.76	6.36	7.66	5.90	6.28	8.03	6.55	7.33	6.62	6.38	6.91
MnO	0.11	0.44	0.28	0.56	0.25	0.51	0.32	0.2	0.29	0.17	0.18	0.26
MgO	0.63	0.83	2.23	2.34	1.76	2.55	2.02	2.24	2.05	2.49	1.90	2.52
CaO	0.023	0.01	0.007	0.045	0.029	0.013	0.106	0	0.05	0	0.006	0
Na_2O	0.03	0.12	0.239	0.26	0.25	0.19	0.17	0.17	0.32	0.18	0.166	0.135
K_2O	10.45	10.53	10.59	9.96	10.51	10.05	9.87	10.64	10.23	10.46	10.69	10.67
F	5.198	5.004	5.895	5.605	5.361	5.724	5.71	6.094	6.379	6.229	6.091	6.208
Li_2O*	3.75	3.12	3.93	3.87	4.13	3.76	3.87	4.15	4.02	4.14	4.20	3.80
H_2O*	1.89	1.85	1.65	1.79	1.95	1.67	1.69	1.58	1.44	1.53	1.62	1.51
Subtotal	103.54	100.62	103.86	104.20	104.03	102.33	103.07	104.39	104.74	104.73	105.14	104.61
O = F. Cl	2.19	2.11	2.48	2.36	2.26	2.41	2.40	2.57	2.69	2.62	2.56	2.61
Total wt.%	101.35	98.52	101.38	101.84	101.77	99.92	100.67	101.82	102.05	102.11	102.57	101.99
Si	6.38	6.26	6.33	6.30	6.36	6.33	6.38	6.40	6.35	6.37	6.37	6.26
Al iv	1.61	1.73	1.66	1.69	1.63	1.66	1.61	1.59	1.64	1.62	1.62	1.73
Al vi	2.26	2.41	2.39	2.32	2.47	2.38	2.30	2.35	2.32	2.34	2.38	2.34
Ti	0.01	-	0.02	-	0.01	-	0.01	-	0.02	-	0.04	0.03
Fe	1.27	1.15	0.71	0.86	0.65	0.71	0.91	0.73	0.82	0.74	0.71	0.77
Mn	0.01	0.05	0.03	0.06	0.02	0.05	0.03	0.02	0.03	0.02	0.02	0.03
Mg	0.13	0.17	0.44	0.47	0.35	0.52	0.41	0.45	0.41	0.49	0.37	0.50
Li*	2.07	1.77	2.13	2.09	2.21	2.06	2.12	2.23	2.17	2.22	2.24	2.06
Ca	-	-	-	-	-	-	0.01	-	-	-	-	-
Na	-	0.03	0.06	0.06	0.06	0.05	0.04	0.04	0.08	0.04	0.04	0.03
K	1.83	1.90	1.82	1.71	1.79	1.75	1.71	1.82	1.75	1.78	1.81	1.83
OH*	1.73	1.75	1.48	1.60	1.73	1.52	1.53	1.41	1.28	1.36	1.43	1.35
F	2.26	2.24	2.51	2.39	2.26	2.47	2.46	2.58	2.71	2.63	2.56	2.64
Cl	-	-	-	-	-	-	-	-	-	-	-	-
Total (apfu)	19.624	19.523	19.625	19.617	19.606	19.565	19.589	19.671	19.638	19.666	19.635	19.625

$10^3 ln\alpha = A \times 10^6/T^2 + B \times 10^3/T + C$ (Zhang *et al.* 1994) and $10^3 ln\alpha = 3.38 \times 10^6/T^2 - 3.40$ (Clayton *et al.* 1972), applied to temperatures in the range of 250 to 500°C. The wolframite-quartz pair revealed a temperature range from 309 to 354°C, while the quartz-cassiterite pair showed a range from 422 to 480°C (Tab. 4). However, according to Zheng (1992), the use of the wolframite-quartz pair has a margin of error of ± 15°C for isotopic temperatures above 300°C.

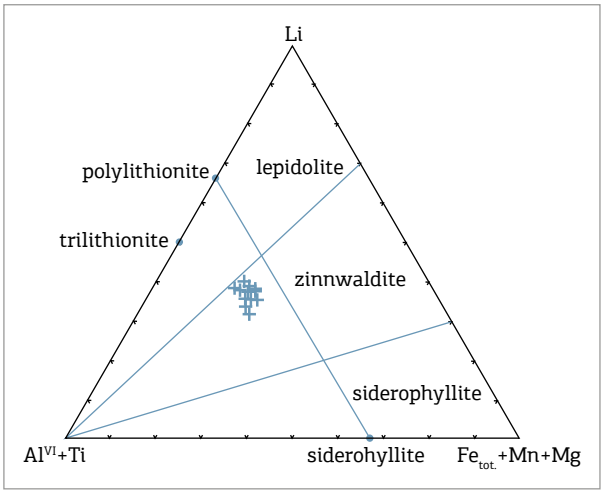

Figure 8. Triangular diagram classification for mica in terms of Li *versus* Al^{VI}+Ti *versus* Fe+Mn+Mg (based on Stone *et al.* 1988).

Given that isotopic fractionation is a direct function of temperature (Taylor Jr. 1978, 1997), the isotopic difference observed between quartz-cassiterite-wolframite suggests that the lowering of the temperature, favored by mixing isotopically different fluids, was the most important factor for the precipitation of cassiterite and wolframite. These data are also consistent with the available isotopic ($\delta^{18}O$) data for the Bom Futuro tin deposit in the Rondônia Tin Province (Souza & Botelho 2009).

Sulphur Isotope ($\delta^{34}S$)

The sulphur isotope studies were focused in part from sulfide mineral assemblage (pyrite, chalcopyrite, sphalerite and molybdenite) from veins, which showed an apparent equilibrium in hydrothermal assemblage. These isotopic results have a degree of uncertainty of ± 0.4‰, which are in Table 4 and are discussed below.

Table 4. Data on the stable isotopes ($\delta^{18}O$ and $\delta^{34}S$) with regard to the wolframite, cassiterite, quartz and some sulfide minerals from greisen and veins. Observe the calculated values for the crystallization temperature ranges for the respective mineral pairs.

Mineral	δ^{18} O (‰)	δ^{34}S (‰)	Mineral pairs	Temperature range (°C)
quartz	9.1	-		
quartz	9.7	-		
wolframite	0.6	-	wolframite + quartz	309 - 354
wolframite	0.9	-		
cassiterite	1.6	-	cassiterite + quartz	422 - 480
cassiterite	1.8	-		
pyrite	-	2.35		
pyrite	-	2.38		
pyrite	-	2.67		
chalcopyrite	-	1.31	chalcopyrite + pyrite	355 - 390
chalcopyrite	-	1.36		
chalcopyrite	-	1.53		
sphalerite	-	1.44	sphalerite + pyrite	416 - 471
sphalerite	-	1.58		
sphalerite	-	1.69		
molybdenite	-	0.52	molybdenite + pyrite	229 - 272
molybdenite	-	0.63		

Pyrite ($\delta^{34}S$ = 2.35‰ – 2.67‰), chalcopyrite ($\delta^{34}S$ = 1.31‰ – 1.53‰), sphalerite ($\delta^{34}S$ = 1.44‰ – 1.69‰) and molybdenite ($\delta^{34}S$ = 0.52‰ – 0.63‰) revealed some degree of variations in the respective sulphur isotope compositions. These variations may be indicative of an isotopic imbalance with a common fluid, probably related to the successive sulfur input in a hydrothermal environment. On the other hand, it is also probable that some of these variations are related to impure samples (*i.e.* micro-inclusions or mineral intergrowth), which may have influenced the accuracy of isotopic analyses. According to Faure (1986), sulfide minerals linked to the hydrothermal phase associated with the evolution of granitic systems shows a wide range of $\delta^{34}S$ values due to the presence of minerals sequentially deposited under different conditions. This complicates isotopic characterization.

Nevertheless, the $\delta^{34}S$ composition range obtained in the sulfide-mineral assemblage (*i.e.* 0.52 to 2.47 ‰), is consistent with an isotopic signature for magmatic fluids, which is between $\delta^{34}S$ = 0‰ - 5‰ (Ohmoto 1972, Rye & Ohmoto 1974). These data are also consistent with the available isotopic ($\delta^{34}S$) data for the Bom Futuro tin deposit in the Rondônia Tin Province (Souza 2003).

The use of $\delta^{34}S$ composition in mineral pairs has also been applied as a geothermometer (Rye & Ohmoto 1974, Ohmoto & Rye 1979). In this context, we chose some mineral pairs (pyrite-sphalerite, pyrite-chalcopyrite and pyrite-molybdenite) for the estimated temperature calculation in the vein systems (Tab. 4), appalling the fractionation equations of Ohmoto & Rye (1979). The choice of pyrite was due to its presence in different phases of sulfation. The results showed an isotopic temperature range from 230 to 471°C for the mineral phases, in which sphalerite is at the highest and molybdenite is at the lowest temperature. These data are also consistent with petrographic observations.

^{40}AR-^{39}AR GEOCHRONOLOGY

^{40}Ar-^{39}Ar geochronological analyses were performed on pure mica (Li-Fe zinnwaldite) crystals that were handpicked from the quartz-topaz-mica greisen with wolframite ± cassiterite collected in the open pit area. The results are in Table 5 and are discussed below.

The step-heating experiments yield a consistent and perfect plateau at the age of 988 ± 5 Ma (Fig. 9), calculated with 90.1% of the total ^{39}Ar released, with MSWD = 0.638 and an analytical error around 3.74%. Ca/K ratio variation measurements indicate discrete different K-bearing phases with the same Ar-Ar age. These ^{40}Ar-^{39}Ar data could imply a cooling or closure time for the late- to post-magmatic processes responsible for the hydrothermal carapace formation and the consecutive polymetallic mineralization in the Igarapé Manteiga deposit.

Therefore, based on available geochronological data on the timing of mineralization in the Rondônia Tin Province

Table 5. ^{40}Ar-^{39}Ar data for Fe-Li zinnwaldite from quartz-topaz-mica greisens (D-647/IG-01 sample).

Power	^{36}Ar/^{40}Ar	^{39}Ar/^{40}Ar	r	Ca/K	%^{40}Atm	%^{39}Ar	^{40}Ar*/^{39}K	Age (Ma)
0.50	0.001131	0.016468	0.003	0.082	33.40	0.20	40.43 ± 2.52	868.7 ± 42.9
0.75	0.000230	0.019587	0.001	0.067	6.80	0.65	47.58 ± 0.92	986.7 ± 14.7
1.00	0.000045	0.020385	0.001	0.023	1.34	2.66	48.40 ± 0.60	999.7 ± 9.6
1.25	0.000005	0.020665	0.000	0.010	0.16	6.39	48.31 ± 0.45	998.4 ± 7.2
< 1.50	0.000008	0.020877	0.000	0.044	0.22	9.31	47.79 ± 0.49	990.1 ± 7.8
< 1.75	0.000007	0.020808	0.000	0.041	0.22	10.72	47.95 ± 0.55	992.6 ± 8.7
< 2.00	0.000002	0.020802	0.000	0.002	0.05	8.52	48.05 ± 0.59	994.2 ± 9.5
< 2.25	0.000009	0.020809	0.000	0.034	0.26	9.76	47.93 ± 0.47	992.3 ± 7.5
< 2.50	0.000012	0.020749	0.000	0.024	0.37	6.44	48.02 ± 0.55	993.7 ± 8.7
< 3.00	0.000010	0.021032	0.000	0.039	0.31	10.41	47.40 ± 0.50	983.8 ± 8.0
< 3.50	0.000008	0.020950	0.001	0.096	0.24	13.34	47.62 ± 1.06	987.3 ± 16.9
< 4.00	0.000001	0.020954	-0.000	0.021	0.02	1.88	47.72 ± 0.61	988.9 ± 9.8
< 5.00	-0.000000	0.021008	-0.000	0.047	-0.01	0.80	47.60 ± 0.88	987.1 ± 14.1
< 7.00	0.000032	0.020894	0.003	0.045	0.94	18.93	47.41 ± 0.83	984.0 ± 13.3

(Tab. 1), this ^{40}Ar-^{39}Ar age correlates the W-Sn Igarapé Manteiga deposit to late-stage rapakivi magmatic phases from the Rondônia Intrusive Suite.

DISCUSSION

Generally, the granites associated with Sn-W deposits, known as tin specialized granites, are the latest, geochemically anomalous and most highly evolved intrusive phases in the composition of magmatic suites (Taylor 1979, Lehmann 1982, Strong 1985, Plimer 1987, Marignac & Cuney 1991, Burnham 1997, Haapala 1997). In the Rondônia Tin Province, the most significant polymetallic concentrations are mainly associated with the Rondônia Intrusive Suite (995-991 Ma). These polymetallic concentrations are normally encapsulated in greisen, veins, breccia and pegmatite bodies, formed during hydrothermal process that occurred in the final stages of the crystallization of highly fractionated granitic phases, such as Li-mica±topaz-albite porphyry granite petrographic type (Leite Jr. 2002, Souza 2003, Sparrenberger 2003, Bettencourt *et al.* 2005a, CPRM 2007). According to Nascimento (2010), in the Igarapé Manteiga W-Sn deposit, the topaz-albite porphyry granite is the highly fractionated magmatic phase, which is linked to the hydrothermal phase responsible for mineralization.

There is extensive literature on specialized granites and the physical-chemical conditions for Sn-W-Nb-Ta extraction, transport and precipitation (Groves & McCarthy 1978, Sillitoe 1985, Pollard & Taylor 1986, Heinrich 1990, Taylor & Wall 1992, Hedenquist & Lowenstern 1994). In general, the formation of these metallic deposits involves fluid encapsulation and a long history of hydrothermal activity exsolved from the residual melt initially undersaturated in water. This fluid phase exsolved beneath the carapace within the cupola may favor effective, complex and protracted metasomatic alteration activities (*i.e.*, greisenization), whose mineral products are the result of the fluid-wall rock interaction processes (Shcherba 1970a, 1970b, Stemprok 1987). Greisenization achieved in aluminosilicate host rocks normally involves the destruction of Fe-micas and feldspar by base-leaching reactions, followed by the precipitation of quartz, muscovite, (F-Li)micas, F-minerals (fluorite, topaz), (Ca-Fe)carbonates (calcite, siderite) and ore minerals (cassiterite, wolframite, sulfides, tourmaline, hematite, Nb-Ta minerals). This process occurs at the temperature range of 200-500°C, at a depth between 2-4 km and in a neutral to alkaline (pH = 6 - 8 or pH ≥ 8) environment, with important participation of halogen complexes (*e.g*, F and Cl) for metals transport (Shcherba 1970a, Plimer 1987, Taylor & Wall 1993, Heinrich *et al.* 1996). Additionally, the increasing internal pressures of the fluid phase may still propagate fractures that result in instantaneous fluidal expansion (*i.e.*, hydrothermal explosion) to form breccia and vein systems. This process may occur in multiple stages of fluidal release and circulation, metasomatic alteration and cyclical mineral precipitation (Eadington 1983, Plimer 1987, Audtat *et al.* 2000).

The petrographic, mineral chemistry and isotopic ($\delta^{18}O$ and $\delta^{34}S$) information presented in this study allows us to propose a paragenetic hydrothermal sequence for greisen and veins from the Igarapé Manteiga W-Sn deposit (Fig. 10). The first stage, at a higher temperature (T > 400°C), was mainly characterized by gangue mineral precipitation, but with ore minerals and some earlier sulfide-mineral phase (sphalerite and pyrrhotite) contribution to the greisen. In the intermediate stage, with a lowering of the temperature (T = 400 - 300°C), the main phase for sulfides precipitation and ore minerals occurred, as well as some gangue minerals (siderite, fluorite, hematite, xenotime) in the greisen and veins. In this phase, exsolution and replacement reactions also occurred, represented by Nb-Ta-Fe oxide minerals exsolved in wolframite and by pyrrhotite with borders replaced by pyrite I. In the final phase, at temperatures ≤ 300°C, precipitation of latter sulfides (bismuthinite, molybdenite, pyrite II) mainly in veins, as well as the Bi- and Ag-tellurides identified by Pereira *et al.* (2008) occurred. These petrographic features suggest successive stages of sulphur supply (*i.e.*, sulphidation),

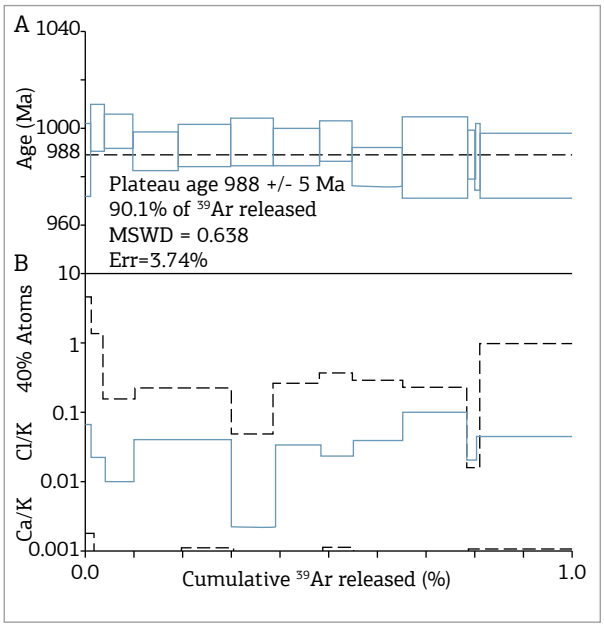

Figure 9. ^{40}Ar-^{39}Ar age spectra for Li-Fe zinnwaldite crystals from quartz-topaz-mica greisen of the Igarapé Manteiga W-Sn deposit. (A) Plateau age calculated (988 Ma) and marked with dotted line; (B) Ca/K and Cl/K ratio measurements.

mainly characterized by different pyritic phases associated with hydrothermal cooling. This interpretation is consistent with sulfur isotope data.

During this hydrothermal cycle, different fluids are normally chaotically mixed (*e.g.* hydrothermal/meteoric) into a modified hydrothermal solution composition, the temperature cools, the isotopic equilibrium and halogen complexes are broken, as well as the pH and Eh conditions are modified to favor the precipitation of metals (Jackson & Helgeson 1985, Taylor & Wall 1993, Heinrich *et al.* 1996). In this context, oxygen isotope data on cassiterite-wolframite-quartz pairs indicate that wolframite precipitated after cassiterite and that the lowering temperature, favored by mixing of isotopically different fluids, was the most important factor for the precipitation of these ore minerals. Additionally, electron microprobe data reveals that Fe^{2+}-rich wolframite have Nb_2O_5 + Ta_2O_5 content that is around 1 wt.%, while cassiterite have Nb_2O_5 + Ta_2O_5 content up to 3 wt.%, in the Fe-rich growth-darker zones (Tab. 2). This is indicative that the hydrothermal fluid phase associated with wolframite precipitation had a lower Nb and Ta content than the fluid phase associated with cassiterite precipitation. This is probably due to the change in composition of fluid phases (oxidized at the beginning and reduced after) associated with lowering temperature.

In general, this information is consistent with the oxygen and deuterium isotope data, as well as with fluid inclusion studies, available on greisen from the Rondônia Tin Province, which indicate a process of mixing fluids during the rise of the hydrothermal stage and ore mineral precipitation (Leite Jr. 2002, Souza 2003, Souza & Botelho 2009, Bettencourt *et al.* 2005a).

The ^{40}Ar-^{39}Ar geochronological analyses yielded an age of 988 ± 5 Ma on a consistent and perfect plateau with negligible Ca/K and Cl/K ratios variation. These data indicate that no abrupt thermal changes occurred that would have led to the loss of Ar radiogenic, and that the hydrothermal environment remained hot for a long time, at around 300 - 350°C, in so far as the Li-Fe zinnwaldite analyzed present a critical temperature for Ar retention around 350°C (Faure 1986, Richards & Noble 1998).

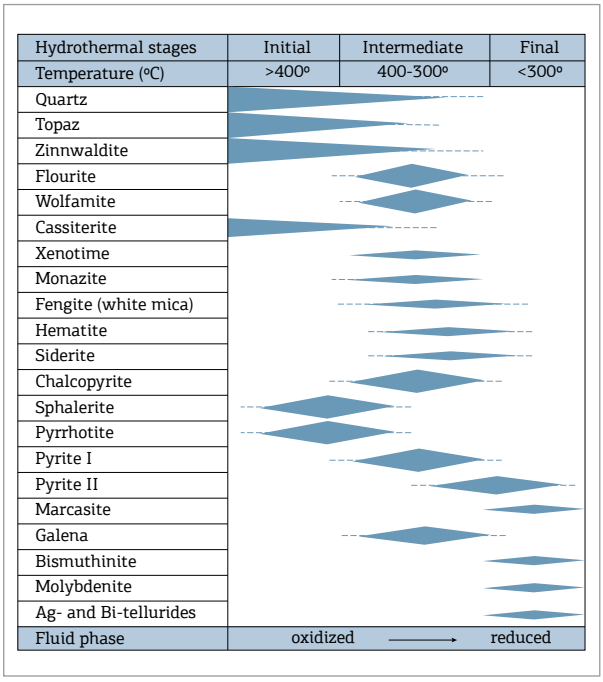

Figure 10. Schematic sequence of the crystallization of the hydrothermal mineral assemblage in the greisen and vein.

CONCLUSIONS

The data presented in this study, in association with information available in regional literature, led us to the following conclusions about the W-Sn Igarapé Manteiga deposit:

- The hydrothermal phase, which is responsible for mineralization, had a cooling time of around 988 Ma, and was linked to the final stages of the crystallization of a highly fractionated granitic phase, which is represented by topaz-albite porphyry granite. This magmatic phase is linked to the Rondônia Intrusive Suite (995-991 Ma);
- This hydrothermal phase was cyclical and protractedly active at temperatures between 300 and 500°C (*i.e.* multiple stages of fluid release), and promoted continuous fluidal circulation, sulphidation, alteration/mineral precipitation (metasomatic replacement = greisenization), followed by hydrofracturing (vein-veinlets and breccia generation);
- Lowering temperature and changes in physico-chemical parameters (fO_2, pressure, Ph, Eh) in the hydrothermal environment, mainly due to the interaction between distinct fluids (hydrothermal *vs* meteoric), were the main determinants for the metal precipitation sequence. These parameters also controlled the atomic substitution mechanisms and exsolution products identified in ore-minerals;
- Relatively, cassiterite occurs earlier than wolframite. Cassiterite precipitated in an oxidized fluid phase with a higher Nb-Ta content and little presence of sulfide, while wolframite precipitated in a reduced fluid phase with a lower Nb-Ta content and a higher presence of sulfide minerals; and
- The main crystallization temperature range for ore-minerals in greisen (wolframite and cassiterite) is estimated between 330 and 430°C, while for sulfide-mineral assemblage in veins and final greisenization the range would be 250 - 350°C.

ACKNOWLEDGEMENTS

This research was financially supported by the Brazilian National Council of Technological and Scientific Development (CNPq), through the CT-Amazonian project (MCT/CNPq nº 575520/2008-6). We thank the Brazilian Coordination for Improvement of Higher Education Personnel (CAPES) for the scholarship granted to the first author. The authors are grateful to geologist Vital Wanderley (METALMIG Mining Company) and to CPRM – Brazilian Geological Survey (Rondônia) for support for field work. A special thanks to anonymous reviewers for appropriate comments that helped improve the final text.

REFERENCES

Alderton D.H.M. 1989. Oxygen isotope fractionation between cassiterite and water. *Mineralogical Magazine*, **53**(371):373-376.

Audtat A., Günther D., Heinrich C.A. 2000. Magmatic-hydrothermal evolution in a fractionating granite: A microchemical study of the Sn-W-F-mineralized Mole Granite (Australia). *Geochimica et Cosmochimica Acta*, **64**(19):3373-3393.

Barton P.B. & Skinner B.J. 1979. Sulfide mineral stabilities. *In*: Barnes H.L. (ed), *Geochemistry of Hydrothermal Ore Deposits*. 2nd ed., Wiley-Interscience, New York, 512p.

Bender K.M., Bühn B.M., Mota-e-Silva J, Chaves J.G.S. 2007. $^{32}S/^{34}S$ isotope analyses by laser ablation MC–ICPMS: method and application. In: *VI South American Symposium on Isotope Geology*, San Carlos de Bariloche. CD-ROM.

Bettencourt J.S., Tosdal R.M., Leite Jr. W.B., Payolla B.L. 1999. Mesoproterozoic rapakivi granites of the Rondônia Tin Province, southwestern border of the Amazonian craton, Brazil – I. Reconnaissance U-Pb geochronology and regional implications. *Precambrian Research*, **95**:41-67.

Bettencourt J.S., Leite Jr. W.B., Goraieb C.L., Sparrenberger I., Bello R.M.S., Payolla B.L. 2005a. Sn-polymetallic greisen-type deposits associated with late-stage rapakivi granites, Brazil: Fluid inclusion and stable isotope characteristics. *Lithos*, **80**(1-4):363-386.

Bettencourt J.S., Sparrenberger I., Leite Jr. W.R., Payolla B.L., Onoe A.T., Tosdal R. M. 2005b. $^{40}Ar/^{39}Ar$ step heating laser system dating of zinnwaldite and muscovite from tin deposits of the Rondônia Tin Province, Brazil: evidence for multiple mineralization episodes. In: *Iº Simpósio Brasileiro de Metalogênese*, MME/SBG/SEG, Gramado, CD-ROM.

Bettencourt J. S., Payolla B.L., Tosdal R.M., Wooden J.L., Leite Júnior W.R., Sparrenberger I. 2006. SHRIMP-RG U-Pb zircon geochronology of gneiss from the Rio Crespo Intrusive Suite, SW Amazonian craton, Rondônia, Brazil: New insight about protolith crystallization and metamorphic ages. In: *V South American Symposium on Isotope Geology*, Medellín, p. 49.

Bettencourt J.S., Leite Jr. W.B., Ruiz A.S., Matos R., Payolla B.L., Tosdal R.M. 2010. The Rondonian-San Ignacio Province in the SW Amazonian Craton: An overview. *Journal of South American Earth Sciences*, **29**(1):28-46.

Burnham C.W. 1997. Magmas and hydrothermal fluids, *In*: Barnes, H.L. (Ed.), *Geochemistry of Hydrothermal Ore Deposits*, **3rd** edition. John Wiley and Sons, New York, pp. 63–123.

Campbell A.R., Rye D., Petersen U. 1984. A hydrogen and oxygen isotope study of the San Cristobal Mine, Peru; implications of the role of water to rock ratio for the genesis of wolframite deposits. *Economic Geology*, **79**(8):1818-1832.

Černý P. & Ercit T.S. 2005. The classification of granitic pegmatites revisited. *The Canadian Mineralogist*, **43**(6):2005-2026.

Chareev D.A., Voronin M.V., Osadchii E.G. 2014. Thermodynamic study of monoclinic pyrrhotite in equilibrium with pyrite in the Ag-Fe-S system by solid-state electrochemical cell technique. *American Mineralogist*, **99**(10):2031-2034.

Clayton R.N., O'Neil J.R., Mayeda T.K. 1972. Oxygen isotope exchange between quartz and water. *Journal of Geophysical Research*, **77**(17):3057-3067.

Costi H.T., Horbe A.M.C., Borges R.M.K., Dall'Agnol R., Rossi A., Sighnolfi G. 2000. Mineral chemistry of cassiterites from Pitinga Province, Amazonian Craton, Brazil. *Revista Brasileira de Geociências*, **30**(4):775-782.

CPRM. 2007. Geologia e recursos minerais do Estado de Rondônia: Sistema de Informações Geográficas – SIG. *Texto Explicativo do Mapa Geológico e de Recursos Minerais do Estado de Rondônia – Escala 1:1.000.000.* – Porto Velho: CPRM. 153p., CD-ROM.

Dalrymple G.B., Alexander Jr. E.C., Lanphere M.A., Kraker G.P. 1981. Irradiation of samples for $^{40}Ar/^{39}Ar$ dating using the Geological Survey TRIGA Reactor, U.S. Geological Survey, *Professional Paper*, n. 1176, 55 p.

Eadington P.J. 1983. A fluid inclusion investigation of ore formation in a tin-mineralized granite, New England, New South Wales. *Economic Geology*, **78**(6):1204-1221.

Fallick A.E., Macaulay C.I., Haszeldine R.S. 1993. Implications of linearly correlated oxygen and hydrogen isotopic compositions for kaolinite and illite in the Magnus sandstone, North Sea. *Clays and Clay Minerals*, **41**(2):184-190.

Faure G. 1986. *Principles of isotopic geology*. John Wiley & Sons, New York. 2nd. 589p.

Foxford K.A., Nicholson R., Polya D.A., Hebblethwaite R.P.B. 2000. Extensional failure and hydraulic valving at Minas da Panasqueira, Portugal: Evidence from vein spatial distributions, displacements and geometries. *Journal of Structural Geology*, **22**(8):1065-1086.

Giuliani G. 1987. La cassitérite zonée du gisement de Sokhret Allal (Granite des Zaër; Maroc Central): Composition chimique et phases fluides associées. *Mineralium Deposita*, **22**(4):253-261.

Groves D.I. & McCarthy T.S. 1978. Fractional Crystallization and the origin of tin deposits in granitoids. *Mineralium Deposita*, **13**(1):11-26.

Guha J., Archambault G., Leroy J. 1983. A correlation between the evolution of mineralizing fluid and the geomechanical development of a shear zone as illustrated by the Hendersin 2 Mine, Québec. *Economic Geology*, **78**(8):1605-1618.

Haapala I. 1997. Magmatic and postmagmatic processes in tin-mineralized granites: topaz-bearing leocogranite in the Eurajoki rapakivi granite stock, Finland. *Journal of Petrology*, **38**(12):1645-1659.

Hedenquist J.W. & Lowenstern J.B. 1994. The role of magmas in the formation of hydrothermal ore deposits. *Nature*, **370**:519-527.

Heinrich C.A. 1990. The chemistry of hydrothermal tin(-tungsten) ore deposition. *Economic Geology*, **85**(3):457-481.

Heinrich C.A., Walshe J.L., Harrold B.P. 1996. Chemical mass transfer modelling of ore-forming hydrothermal systems: Current practise and problems. *Ore Geology Reviews*, **10**(3-6):319-338.

Higgins N.C. & Kerrich R. 1982. Progressive ^{18}O depletion during CO_2 separation from a carbon dioxide-rich hydrothermal fluid: evidence from the Grey River tungsten deposit, Newfoundland. *Canadian Journal of Earth Sciences*, **19**(12):2247-2257.

Hsu L.C. 1976. The stability relations of the wolframite series. *American Mineralogist*, **61**(9-10):944-955.

Isotta C.A.L., Carneiro J.M., Kato H.T., Barros R.J.L. 1978. *Projeto Província Estanífera de Rondônia:* relatório final. MME/DNPM/CPRM, Porto Velho (RO), vol. I, 407p.

Ivanova G. 1988. Geochemical conditions of formation of various composition wolframites. *Bulletin of Mineralogy*, **111**:97-103.

Jackson K.J. & Helgeson H.C. 1985. Chemical and thermodynamic constraints on the hydrothermal transport and deposition of tin: I. Calculation of the solubility of cassiterite at high pressures and temperatures. *Geochimica et Cosmochimica Acta*, **49**(1):1-22.

Jébrak M. 1997. Hydrothermal breccias in vein-type ore deposits: A review of mechanisms, morphology and size distribution. *Ore Geology Reviews*, **12**(3):111-134.

Jensen M.L. & Bateman A.M. 1981. *Economic mineral deposits: revised printing*. John Wiley & Sons Ed., New York, 3nd edition, 593p.

Kelly W.C. & Rye R.O. 1979. Geologic, fluid inclusion, and stable isotope studies of the tin-tungsten deposits of Panasqueira, Portugal. *Economic Geology*, **74**(8):1721-1822.

Kissin S.A. & Scott S.D. 1982. Phase relations involving pyrrhotite below 350 degrees C. *Economic Geology*, **77**(7):1739-1754.

Kloosterman J.B. 1968. Uma província do tipo nigeriano no sul da Amazônia. *Revista de Engenharia, Mineração e Metalurgia. Rio de Janeiro*. XLVII **(278):**59-64 e XLVII **(280):**167-168.

Laznicka P. 1989. Breccias and ores. Part 1: History, organization and petrography of breccias. *Ore Geology Reviews*, **4**(4):315-344.

Leal J.W.L., Silva G.H., Santos D.B., Teixeira W., Lima M.I.C., Fernandes C.A.C., Pinto A.C. 1978. *Levantamento de Recursos Naturais: Folha SC.20 Porto Velho (I – Geologia)*. MME/DNPM. Projeto RADAMBRASIL, Rio de Janeiro, v.**16:**19-184.

Leite Jr. W.B., Payolla B.L., Betttencourt J.S., Tassinari C.C.G. 2001. New K-Ar ages of the primary tin mineralization in the Rondônia Tin Province, Brazil. *In:* III South American Symposium on Isotope Geology (SSAGI), Pucon-Chile, CD-ROM, **5:** 484-487.

Leite Jr. W.B. 2002. *A Suíte Intrusiva Santa Clara (RO) e a mineralização primária polimetálica (Sn,W, Nb, Ta, Zn, Cu e Pb) associada*. Tese de Doutorado, Instituto de Geociências, Universidade de São Paulo, São Paulo, 247p.

Lehmann B. 1982. Metallogeny of tin; magmatic differentiation versus geochemical heritage. *Economic Geology,* **77**(1):50-59.

Lenharo S.L.R., Pollard P.J., Born H. 2003. Petrology and textural evolution of granites associated with tin and rare-metals mineralization at the Pitinga mine, Amazonas, Brazil. *Lithos*, **66**(1-2):37-61.

Liu X., Xing H., Zhang D. 2015. The mechanisms of the infill textures and its implications for the five-floor zonation at the Dajishan vein-type tungsten deposit, China. *Ore Geology Reviews*, **65**(1):365-374.

Lowell G.R. & Ahl M. 2000. Chemistry of dark zinnwaldite from Bom Futuro tin mine, Rondônia, Brazil. *Mineralogical Magazine*, **64**(4):699-709.

Macaulay C.I, Fallick A.E, Haszeldine R.S, Graham C.M. 2000. Methods of laser-based stable isotope measurement applied to diagenetic cements and hydrocarbon reservoir quality. *Clay Minerals*, **35**(1):313-322.

Marignac C. & Cuney M. 1991. What is the meaning of granite specialization for Sn, W deposit genesis? *In*: M. Pagel & J.L. Leroy (Edt.): *Source, transport and deposition of metals*. Balkema, Rotterdam: 771-774.

McDougall I. & Harrison T.M. 1988. *Geochronology and Thermochronology by the $^{40}Ar/^{39}Ar$ Method*. Oxford University Press, New York, 212 p.

METALMIG 2008. Projeto Igarapé Manteiga: Avaliação e Recomendações. *Relatório técnico interno*, 47p. e anexos (mapas).

Möller P., Dulski P., Szacki W., Malow G., Riedel E. 1988. Substitution of tin in cassiterite by tantalum, niobium, tungsten, iron and manganese. *Geochimica et Cosmochimica Acta*, **52**(6):1497-1503.

Murciego A., Sanchez A.G., Dusausoy Y., Pozas J.M.M., Ruck R. 1997. Geochemistry and EPR of cassiterites from the Iberian Hercynian Massif. *Mineralogical Magazine*, **61**:357-365.

Murowchick J.B. & Barnes H.L. 1986. Marcasite precipitation from hydrothermal solutions. *Geochemica et Cosmochemica Acta*, **50**(12):2615-2629.

Murowchick J.B. 1992. Marcasite inversion and the petrographic determination of pyrite ancestry. *Economic Geology*, **87**(4):1141-1152.

Nascimento T.M.F. 2010. *Depósito W-Sn Igarapé Manteiga: geologia e metalogênese*. Dissertação de Mestrado, Programa de Pós-graduação em Geociências, Universidade Federal do Amazonas, Manaus, 93p.

Neiva A.M.R. 1996. Geochemistry of cassiterite and its inclusions and exsolutions products from tin and tungsten deposits in Portugal. *The Canadian Mineralogist*, **34**:745-768.

Neiva A.M.R. 2008. Geochemistry of cassiterite and wolframite from tin and tungsten quartz veins in Portugal. *Ore Geology Reviews*, **33**(3-4):221-238.

Ohmoto H. 1972. Systematics of sulfur and carbon isotopes in Hydrothermal Ore Deposits. *Economic Geology*, **67**(5):551-578.

Ohmoto H. & Rye R.O. 1979. Isotopes of sulfur and carbon. In: H. L. Barnes (Edt.). *Geochemistry of hydrothermal ore deposits*. John Wiley & Sons, New York, 2nd., (10):509-567.

Ohmoto H. & Lasaga A.C. 1982. Kinetics of reactions between aqueous sulfates and sulfides in hydrothermal systems. *Geochimica et Cosmochimica Acta*, **46**(10):1727-1745.

Payolla B.L., Bettencourt J. S., Kozuch M., Leite Jr. W.B., Fetter A.H., Van Schmus R. 2002. Geological evolution of the basement rocks in the east-central part of the Rondônia Tin Province, SW Amazonian Craton, Brazil: U-Pb and Sm-Nd isotopic constraints. *Precambrian Research*, **119:**141-169.

Pereira R.M., Neumann R., Castro C.C., Wanderley V.J.R. 2008. A mina de wolframita do Igarapé Manteiga, Rondônia: uma abordagem preliminar. In: 44º Congresso Brasileiro de Geologia, SBG, Curitiba, *Anais*, p. 959.

Phillips W.J. 1972. Hydraulic fracturing and mineralization. *Journal of the Geological Society of London*, **128**:337-359.

Plimer I.R. 1987. Fundamental parameters for the formation of granite-related tin deposits. *Geologische Rundschau*, **76**(1):23-40.

Pollard P.J. & Taylor R.G. 1986. Progressive evolution of alteration and tin mineralization: Controls by interstitial permeability and fracture-related tapping of magmatic fluid reservoirs in tin granites. *Economic Geology*, **81**(7):1795-1800.

Polya D.A. 1988. Compositional variation in wolframites from the Barroca Grande mine, Portugal: Evidence for fault-controlled ore formation. *Mineralogical Magazine*, **52**(367):497-503.

Priem H.N.A., Boelrijk N.A.I.M., Hebeda E.H., Verschure R.H., Bom E.H. 1966. Isotopic age of tin granites in Rondônia, N.W. Brazil. *Geologie en Mijnbouw*, **45:**191-192.

Priem H.N.A., Boelrijk N.A.I.M., Hebeda E.H., Verdurmen E.A.Th., Verschure R.H., Bon E.H. 1971. Granitic complexes and associated tin mineralizations of "Grenville" age in Rondônia, Western Brazil. *Geological Society of America Bulletin*, **82:**1095-1102.

Qian G., Xia F., Brugger J., Skinner W.M., Bei J., Chen G., Pring A. 2011. Replacement of pyrrhotite by pyrite and marcasite under hydrothermal conditions up to 220°C: An experimental study of reaction textures and mechanisms. *American Mineralogist*, **96**:1878-1893.

Richards J.P. & Noble S.R. 1998. Application of radiogenic isotope systems to the timing and origin of hydrothermal processes. *In*: J.P. Richards & P.B. Larson (Edt.). *Techniques in hydrothermal ore deposits geology*. Reviews in Economic Geology, v.10, ch.9, pp.195-233.

Richards J.P. 2011. Magmatic to hydrothermal metal fluxes in convergent and collided margins. *Ore Geology Reviews*, **40**(1):1-26.

Rieder M., Cavazzini G., D'Yakonov Y.S., Frank-Kamenetskii V.A., Gottardi G., Guggenheim S., Koval P.V., Müller G., Neiva A.M.R., Radoslovich E.W., Robert J-L., Sassi F.P., Takeda H., Weiss Z., Wones D.R. 1998. Nomenclature of the micas. *Clays and Clay Minerals*, **46**(5):586-595.

Roddick J.C. 1983. High precision intercalibration of $^{40}Ar/^{39}Ar$ standards. *Geochimica et Cosmochimica Acta*, **47**(5):887-898.

Rye R.O. & Ohmoto H. 1974. Sulfur and carbon isotopes and ore genesis: A review. *Economic Geology*, **69**(6):826-842.

Santos J.O.S., Hartmann L.A., Gaudette H.E., Groves D.I., Mcnaughton N.J., Fletcher I.R. 2000. A new understanding of the provinces of the Amazon Craton based on integration of field mapping and U-Pb and Sm-Nd geochronology. *Gondwana Research*, **3**(4):453-488.

Santos J.O.S., Rizzotto G.J., Potter P.E., McNaughton N.J., Matos R.S., Hartmann L.A., Chemale Jr. F., Quadros M.E.S. 2008. Age and autochthonous evolution of the Sunsás Orogen in West Amazon Craton based on mapping and U–Pb geochronology. *Precambriam Research*, **165**(3-4):120-152.

Santos Jr., P.S.M. 2015. *Metalogênese do depósito estanífero Liberdade, Campo Novo de Rondônia – RO*. Dissertação de Mestrado, Instituto de Geociências, Universidade de Brasília, nº 345, 87p.

Scandolara J.E. 2006. *Geologia e evolução do Terreno Jamari, embasamento da faixa Sunsás/Aguapeí, centro-leste de Rondônia, sudoeste do Cráton Amazônico*. Tese de Doutorado, Instituto de Geociências, Universidade de Brasília, 384p.

Scandolara J.E., Fuck R.A., Dantas E.L., Souza V.S. 2013. Geochemistry of Jamari Complex, central-eastern Rondônia: Andeantype magmatic arc and Paleoproterozoic crustal growth of the southwestern Amazonian Craton, Brazil. *Journal of South American Earth Sciences*, **46**:35-62.

Schwartz M.O. 1992. Geochemical criteria for distinguishing magmatic and metasomatic albite-enrichment in granitoids – examples from the Ta-Li granite Yichun (China) and the Sn-W deposit Tikus (Indonesia). *Mineralium Deposita*, **27**(2):101-108.

Seward T.M. & Branes H.L. 1997. Metal transport by hydrothermal ore fluids. *In*: H.L. Barnes (ed.). *Geochemistry of Hydrothermal Ore Deposits*, **3rd** ed., John Wiley and Sons, New York, pp. 435–486.

Shcherba G.N. 1970a. Greisens (part 1). *International Geology Review*, **12**(2):114-255.

Shcherba G.N. 1970b. Greisens (part 2). *International Geology Review*, **12**(3):239-255.

Sillitoe R.H. 1985. Ore-related breccias in vulcanoplutonic arcs. *Economic Geology*, **80**(6):1465-1514.

Silva J.M., Ferreira Filho C.F., Bühn B., Dantas E.L. 2011. Geology, petrology and geochemistry of the "Americano do Brasil" layered intrusion, central Brazil, and its Ni–Cu sulfide deposits. *Mineralium Deposita*, **46**:57-90.

Souza E.C., Melo A.F.F., Adamy A., Soeiro R.S., Daleiro V. 1975. *Projeto nordeste de Rondônia:* relatório final. MME/DNPM/CPRM, Brasília, v.1, 225p.

Souza V.S. 2003. *Evolução magmática e modelo metalogenético do sistema vulcano-plutônico estanífero Bom Futuro (RO)*. Tese de Doutorado. Instituto de Geociências, Universidade de Brasília, Brasília, 240p.

Souza V.S., Teixeira L.M., Botelho N.F. 2005. Datação U-Th-Pb de monazita hidrotermal e sua aplicação na geocronologia da mineralização de estanho em zonas de greisen do sistema granítico Palanqueta, depósito de estanho do Bom Futuro (RO). *Revista Brasileira de Geociências*, **35**(1):43-48.

Souza V.S., Teixeira L.M., Dantas E.L. Botelho N.F., Laux J.H. 2006. Idades U-Th-Pb e U-Pb em monazita de ortognaisse do Complexo Jamari, área do depósito de estanho de Bom Futuro (RO). *Revista Brasileira de Geociências*, **36**(1):71-76.

Souza V.S. & Botelho N.F. 2009. Composição química e isótopos de oxigênio em cassiterita e wolframita nos greisens do albita granito Palanqueta, depósito de estanho de Bom Futuro (RO). *Revista Brasileira de Geociências*, **39**(4):695-704.

Sparrenberger I. 2003. *Evolução da mineralização primária estanífera associada ao maciço granítico Santa Bárbara, Rondônia*. Tese de Doutorado, Instituto de Geociências, Universidade de São Paulo, São Paulo, 252p.

Stanton R.L. 1972. *Ore petrology*. New York, McGraw-Hill Book, 713p.

Steiger R.H. & Jäger E. 1977. Subcommission on geochronology: Convention on the use of decay constants in geo- and cosmochronology. *Earth and Planetary Science Letters*, **36**(3):359-362.

Stemprok M. 1987. Greisenization (a review). *Geologische Rundschau*, **76**(1):169-175.

Stemprok M. 1991. Ongonite from Ongon Khairkhan, Mongolia. *Mineralogy and Petrology*, **43**(4):255-273.

Stone M., Exley C.S., George M.C. 1988. Compositions of trioctahedral micas in the Cornubian batholith. *Mineralogical Magazine*, **52**:175-192.

Strong D.F. 1985. A review and model for granite-related mineral deposits. *In*: R.P. Taylor & D.F. Strong (Edt.): *Recent advances in the geology of granite-related mineral deposits*. The Canadian Institute of Mining and Metallurgy (Special Volume). 39:424-445

Sun S.S. & Eadington P.J. 1987. Oxygen isotope evidence for the mixing of magmatic and meteoric waters during tin mineralization in the Mole granite, New South Wales, Australia. *Economic Geology*, **82**:43-52.

Taylor Jr. H.P. 1974. The application of oxygen and hydrogen isotope studies to problems of hydrothermal alteration and ore deposition. *Economic Geology*, **69**(6):843-883.

Taylor Jr. H.P. 1978. Oxygen and hydrogen isotope studies of plutonic granitic rocks. *Earth and Planetary Science Letters*, **38**(1):177-210.

Taylor Jr. H.P. 1997. Oxygen and hydrogen isotope relationships in hydrothermal mineral deposits. In: H. L. Barnes (Edt.). *Geochemistry of hydrothermal ore deposits*. John Wiley & Sons, New York, 3nd., p.229-302.

Taylor R.G. 1979. *Geology of tin deposits*. In: developments in economic geology (11). Elsevier Ed. Amsterdam. 543p.

Taylor J.R. & Wall V.J. 1992. The behavior of tin in granitoid magmas. *Economic Geology*, **87**(2):403-420.

Taylor J.R. & Wall V.J. 1993. Cassiterite solubility, tin speciation, and transport in magmatic aqueous phase. *Economic Geology*, **88**(2):437-460.

Tindle A.G. & Webb P.C. 1990. Estimation of lithium contents in trioctahedral micas using microprobe data; application to micas from granitic rocks. *European Journal of Mineralogy*, **2**(5):595-610.

Tohver E., Van der Pluijm B., Mezger K., Scandolara J., Essene E.J. 2005. Two stage tectonic history of the SW Amazon craton in the late Mesoproterozoic: identifying a cryptic suture zone. *Precambrian Research*, **137:**35-59.

Vaughan D.J. & Craig J.B. 1997. Sulfide ore mineral stabilities, morphologies, and intergrowth textures. *In:* H.L. Barnes, (ed.), *Geochemistry of Hydrothermal Ore Deposits*. 3nd ed., John Wiley & Sons, New York, pp.367-434.

Waychunas G.A. 1991. Crystal chemistry of oxides and oxyhydroxides. In: D.H. Lindsley (ed.) *Oxide Minerals: petrologic and magnetic significance*. Mineralogical Society of America, Michigan, *Reviews in Mineralogy*, **25**(2):11-68.

Wood S.A., Crerar D.A., Borcsik M.P. 1987. Solubility of the assemblage purite-pyrrothite-magnetite-sphalerite-galena-Au-stibnite-bismithinite-argentite-molybidenite in H_2O-CO_2-NaCl solution from 200° to 350°C. *Economic Geology*, **82**:1864-1887.

Wood S.A. & Samson I.M. 1998. Solubility of ore minerals and complexation of ore metals in hydrothermal solution. *In*: J.P. Richards and P.B. Larson (Ed.), *Techniques in Hydrothermal Ore Deposits Geology*, Reviews in Economic Geology, SEG-USA, vol.10, ch. 2, pp.33-80.

Yokoi O.Y., Viglio E.P., Waghorn J.G., Jones J.P., Figueroa L.A. 1987. Potosi, a primary tin deposit in Rondônia. *Revista Brasileira de Geociências*, **17**(4):557-561.

Yund R.A. & Hall H.T. 1969. Hexagonal and monoclinic pyrrhotites. *Economic Geology*, **64**(4):420-423.

Zhang L-G, Liu J-X, Chen Z-S, Zhou H-B. 1994. Experimental investigations of oxygen isotope fractionation in cassiterite and wolframite. *Economic Geology*, **89**(1):150-157.

Zheng Y-F. 1992. Oxygen isotope fractionation in wolframite. *European Journal of Mineralogy*, **4**:1331-1335.

Zhu, J-C; Li, R-K; Li, F-C; Xiong, X-L; Zhou, F-Y and Huang, X-L. 2001. Topaz-albite granites and rare-metal mineralization in the Limu District, Guangxi Province, southeast China. *Mineralium Deposita*, **36**(5):393-405.

Available at www.sbgeo.org.br